Optics Communications

Study of the velocity-selection satellites present in the 5P3 / 2 → 6PJ(J = 1/2, 3/2) electric quadrupole transitions in atomic rubidium.

--Manuscript Draft--

Manuscript Number:	
Article Type:	Research Paper
Section/Category:	Atomic and molecular physics
Keywords:	Electric quadrupole transition; selection of velocities; atomic rubidium; rate equations
Corresponding Author:	Jose Jimenez-Mier, Ph. D. National Autonomous University of Mexico Institute of Nuclear Sciences Mexico, MEXICO
First Author:	Jose Jimenez-Mier, Ph. D.
Order of Authors:	Jose Jimenez-Mier, Ph. D.
	Francisco S. Ponciano-Ojeda, PhD
	Cristian Mojica-Casique, PhD
	Lina M. Hoyos-Campo, PhD
	Fernando Ramírez-Martínez, PhD
	Jesus Flores-Mijangos, PhD
Abstract:	This article presents detailed experimental and theoretical studies of the satellite fluorescence lines observed when the 5P3 / 2 → 6PJ, (J = 1/2, 3/2) electric quadrupole transition (E2) is excited in a room temperature vapor of rubidium atoms. The initial state of this E2 transition is prepared by a narrow linewidth laser locked to one of the dominant 5S1 / 2 → 5P3 / 2 D2 hyperfine excitations for zero-velocity atoms. Effects due to the selection of different atomic velocity classes in this preparation step are responsible for the presence of several satellite lines that can be found in the fluorescence decay spectra of both 85Rb and 87Rb. Compared to the main lines, these satellites do not show a strong dependence on the relative linear polarization directions of the lasers used in the preparation and the electric quadrupole steps. The relative intensities of the satellites decrease as the intensity of the preparation laser increases. Results of a rate equation calculation that explicitly includes selection-of-velocity effects indicate that optical pumping plays a central role in determining the relative intensities and the polarization dependence of the satellite lines. When the preparation laser is locked to the 5S1 / 2F1 = 1 → 5P3 / 2F2 = 0 low F cyclic transition in 87Rb, six lines were found in addition to the 5P3 / 2F2 = 0 → 6P3 / 2F3 = 2 lone electric quadrupole transition for zero velocity atoms. In this case, the calculated spectrum is necessary for the correct interpretation of the experimental results, clearly indicating that optical pumping and selection of velocities are responsible for these six additional electric quadrupole lines.
Suggested Reviewers:	Satoshi Tojo, PhD Professor, Chuo University tojo@phys.chuo-u.ac Professor Tojo has made important contributions to the study of electric dipole forbidden transitions.
	Martial Ducloy, PhD Professor, Nanyang Technological University martial.ducloy@ntu.edu.sg Professor Ducloy has recent contributios to teh study of forbidden transitions in alkali atoms.
	Sile Nic Chormaic, PhD Professor, Okinawa Institute of Science and Technology Graduate University sile.nicchormaic@oist.jp Professor Nic Chormaic is an expert in the field, with recent contributions to the study

	of forbidden transitions in atoms.

INSTITUTO DE CIENCIAS NUCLEARES, UNAM
CIRCUITO EXTERIOR C.U. A. POSTAL 70-543 CDMX

February 10, 2023

Optics Communications

In the submitted manuscript “Study of the velocity-selection satellites present in the $5P_{3/2} \to 6P_{J} $ ($J = 1/2, \ 3/2 $) electric quadrupole transitions in atomic rubidium” we make a detailed study of the fluorescence spectra that follow the excitation of the $5P_{3/2} \to 6P_{J} $ electric dipole forbidden transition in atomic rubidium. The results are compared with a rate equation calculation that includes atom-velocity and frequency detuning dependent terms. It is therefore possible to study not only the dominant emission lines, but also the velocity-selection satellite lines, which provide useful and complementary information to the forbidden excitation process. The manuscript also presents for the first time results obtained when the initial states in the transition are the F=0, 1 and 2, low F hyperfine states. In this case the calculation is necessary to identify all forbidden excitations present in the emission spectrum, and it allowed us to categorically conclude the electric quadrupole nature of the forbidden transition.
The authors believe that these results give new and interesting information that make this set of forbidden transitions useful in the control and characterization of quantum states in room temperature atoms. Therefore, we consider that the manuscript can be published in the journal Optics Communications.
This work was funded by DGAPA-UNAM and CONACyT, under the research grants described in section Acknowledgements of the manuscript.
Please contact me if you need more information about the manuscript.

Best regards,

José Jiménez-Mier
Professor

Study of the velocity-selection satellites present in the $5P_{3/2} \rightarrow 6P_J$ ($J = 1/2,\ 3/2$) electric quadrupole transitions in atomic rubidium.

F. S. Ponciano-Ojeda, C. Mojica-Casique, L. M. Hoyos-Campo,
F. Ramírez-Martínez,* J. Flores-Mijangos, and J. Jiménez-Mier†
Instituto de Ciencias Nucleares, UNAM. Circuito Exterior, Ciudad Universitaria, 04510 Ciudad de México, México.

(Dated: February 15, 2023)

Abstract

This article presents detailed experimental and theoretical studies of the satellite fluorescence lines observed when the $5P_{3/2} \rightarrow 6P_J$, ($J = 1/2, 3/2$) electric quadrupole transition (E2) is excited in a room temperature vapor of rubidium atoms. The initial state of this E2 transition is prepared by a narrow linewidth laser locked to one of the dominant $5S_{1/2} \rightarrow 5P_{3/2}$ D2 hyperfine excitations for zero-velocity atoms. Effects due to the selection of different atomic velocity classes in this preparation step are responsible for the presence of several satellite lines that can be found in the fluorescence decay spectra of both ^{85}Rb and ^{87}Rb. Compared to the main lines, these satellites do not show a strong dependence on the relative linear polarization directions of the lasers used in the preparation and the electric quadrupole steps. The relative intensities of the satellites decrease as the intensity of the preparation laser increases. Results of a rate equation calculation that explicitly includes selection-of-velocity effects indicate that optical pumping plays a central role in determining the relative intensities and the polarization dependence of the satellite lines. When the preparation laser is locked to the $5S_{1/2}\ F_1 = 1 \rightarrow 5P_{3/2}\ F_2 = 0$ *low-F* cyclic transition in ^{87}Rb, six lines were found in addition to the $5P_{3/2}\ F_2 = 0 \rightarrow 6P_{3/2}\ F_3 = 2$ lone electric quadrupole transition for zero velocity atoms. In this case, the calculated spectrum is necessary for the correct interpretation of the experimental results, clearly indicating that optical pumping and selection of velocities are responsible for these six additional electric quadrupole lines.

Keywords: Electric quadrupole transition, selection of velocities, atomic rubidium, rate equations

I. INTRODUCTION

Optical transitions beyond the electric dipole approximation play an important role in basic and applied research areas. For example, cosmologists find them useful in understanding the microwave background due to hydrogen and helium recombination in early space [1]. Electric quadrupole (E2) transitions are also used in the search for parity violation in atoms [2, 3]. Long-lived states that may be reached via forbidden transitions are attractive for error correction on quantum bits [4, 5]. E2 transitions have been identified as alternatives to the use of narrow-dipole lines that need to be cleanly excited in lattice-based atomic clocks

* ferama@nucleares.unam.mx

† jimenez@nucleares.unam.mx

[6, 7]. Forbidden transitions have become of interest to measure isotope shifts in ions of calcium [8] and ytterbium [9] that may provide clues for physics beyond the standard model. Recent work is dedicated to the study of forbidden transition in evanescent fields [10, 11], fiber beams [12, 13], structured beams [14, 15], in microcavities [16, 17], in the presence of nanoscale materials [18] or surface plasmons [19, 20]. Forbidden transitions are expected to play an important part in the use of structured light in nonlinear quantum optics [21].

Experiments with forbidden transitions have been performed in cold ions [22] and cold neutral atoms [23–25]. Forbidden transitions are also observed in room temperature or even hot atomic vapors. These atomic vapor experiments study $s \rightarrow d$ transitions in alkali atoms [13, 26, 27] and the strong $p \rightarrow p$ E2 excitation in rubidium [28–32]. The first $p \rightarrow p$ experiment [28] found an anomaly in the fine structure line intensities that was attributed to a significant magnetic dipole contribution in the forbidden transition. This was later disproved in a cold atom experiment [24] that clearly indicated that the $6P \rightarrow 8P$ excitations in rubidium are due to electric quadrupole transitions only. This finding was later confirmed in room temperature experiments with the $5P_{3/2} \rightarrow 6P_{3/2,1/2}$ E2 transitions for both fine structure components of the final state [29, 31]. In this series of papers optical-optical double resonance experiments were performed, with one light field used to prepare zero-velocity atoms in the hyperfine state of the $5P_{3/2}$ manifold with the highest F value (cyclic transition), which was then excited by the E2 transition. This allowed measurements free of Doppler-broadening that resolved the hyperfine structure of both $6P_J$ ($J = 1/2,\ 3/2$) fine structure states. These experiments found strong E2 lines for these zero-velocity atoms, but the spectra also showed weaker satellite transitions. The origin of these satellites was readily identified [29] as being due to E2 transitions that involve other $5P_{3/2}$ hyperfine states that are produced by the preparation step that is resonant with nonzero-velocity atoms in a non-cyclic transition. A model based on the rate equation approximation for the population of the zero-velocity atoms adequately reproduces the intensity distribution of the strongest electric quadrupole transitions seen in a typical spectrum. These transitions were also found to show a strong dependence on the relative polarizations of the light beams used in the preparation step and in the excitation of the E2 transition [30, 31]. Once again, the static rate equation calculation for zero-velocity atoms took good care of recreating the observed polarization dependence of the strongest electric quadrupole transitions. Furthermore, these E2 transitions were shown to be ideal probes of the Autler-Townes splitting caused by the

strong cyclic D2 transition [32]. All these results took advantage of the good signal-to-noise ratio achieved when the hyperfine state with the largest F value is produced in the preparation of the $5P_{3/2}$ manifold.

These works show that the $p \rightarrow p$ electric quadrupole transitions for zero velocity atoms are sensitive, non-perturbing probes of optical pumping effects in room temperature atomic vapors. In particular, the satellite lines are useful for studying in detail the interplay between selection of velocities and optical pumping effects in the preparation step using both cyclic and non-cyclic transitions. These probes of velocity selective optical pumping (VSOP) may be of interest in different areas of current research. VSOP has been used in the development of room-temperature quantum memories [33, 34] or in experiments that use motion-selective coherent population trapping [35] to achieve subrecoil cooling in atomic samples [36, 37]. VSOP is used to study hyperfine optical pumping effects of thermal rubidium atoms probed by an evanescent electromagnetic field [38] and in surface plasmon resonance (SPR) experiments [39]. Also, VSOP is very useful in the construction of narrow optical filters in atom-photon interaction experiments where the signal-to-noise ratio is a critical parameter [40, 41]. Applications, such as free space laser communication and the generation of narrowband quantum light uses these atomic based filters [42, 43].

In this paper we present the results of a detailed study of the satellite lines that are observed in the electric quadrupole spectra. It is shown that more satellites can be found in addition to the single satellite identified in [29]. We follow the dependence of these satellites on the intensity of the preparation light. We also measure the polarization dependence of these satellite lines. A dynamical rate equation calculation in which velocity-dependent terms are included in both preparation and E2 excitations is used to correctly identify all observed satellites. This calculation also accurately describes the intensity and polarization behavior of all the E2 lines. Finally, we present an electric quadrupole spectrum that results by excitation from the $5P_{3/2}F = 0$ (low F cyclic transition) hyperfine state prepared for zero-velocity ^{87}Rb atoms. This is particularly interesting because, in this case, only the transition to the $6P_{3/2}F = 2$ hyperfine state is allowed by the electric quadrupole selection rules. Any other lines present in this spectrum have to result from velocity selection effects or may be an indication of the presence of magnetic dipole transitions.

The rest of the paper is structured as follows. A brief description of the experiment is presented in section II. Then section III outlines the procedure followed to introduce

velocity-dependent terms in the rate equation approximation. Section IV shows the experimental results with the corresponding comparison with the calculation. This includes an E2 spectrum obtained with the preparation laser locked to the low F cyclic transition. Finally, the conclusions are given in section V.

II. EXPERIMENTAL SETUP.

Details of the experimental setup shown in Fig. 1 have been previously presented in references [29–31]. Briefly, the 780 nm preparation beam and the quadrupole exciting beam (911 nm or 917.5 nm) counterpropagate along a 7.5 cm long natural-abundance rubidium absorption cell which is kept at room temperature. The preparation beam is linearly polarized and the direction of its electric field then defines the quantization axis for the atomic system. The quadrupole exciting beam is also linearly polarized, with the polarization direction either parallel or perpendicular to the quantization axis. The polarization direction is set by a half wave plate. The 420 nm fluorescence of atoms decaying from the second excited state is collected by a lens system and then passes through an interference filter before it reaches a photomultiplier tube. The system detects fluorescence emitted at right angles with respect to both the light propagation axis and the polarization direction of the preparation beam. The preparation beam is chopped at a frequency of 800 Hz, and the fluorescence signal is detected in phase with the chopper reference signal. Electric quadrupole fluorescence spectra are then recorded using a digital oscilloscope.

Except for the last set of data presented in this paper, the preparation beam frequency is locked to the $5SF_1 = I + 1 \rightarrow 5P_{3/2}F_2 = F_1 + 1$ cyclic transition, where I is the nuclear spin, and the frequency of the quadrupole exciting beam is scanned. In this paper we also present the results of spectra recorded with the preparation laser locked to the $5S\ F_1 = 1 \rightarrow 5P_{3/2}\ F_2 = 0$ low F cyclic transition in ^{87}Rb.

III. THEORY.

An energy level diagram for atomic rubidium is shown in Fig. 2. Using this diagram one can follow the steps used for the production and the detection of the electric dipole forbidden transition. A preparation laser (780 nm) is used to excite atoms from one of

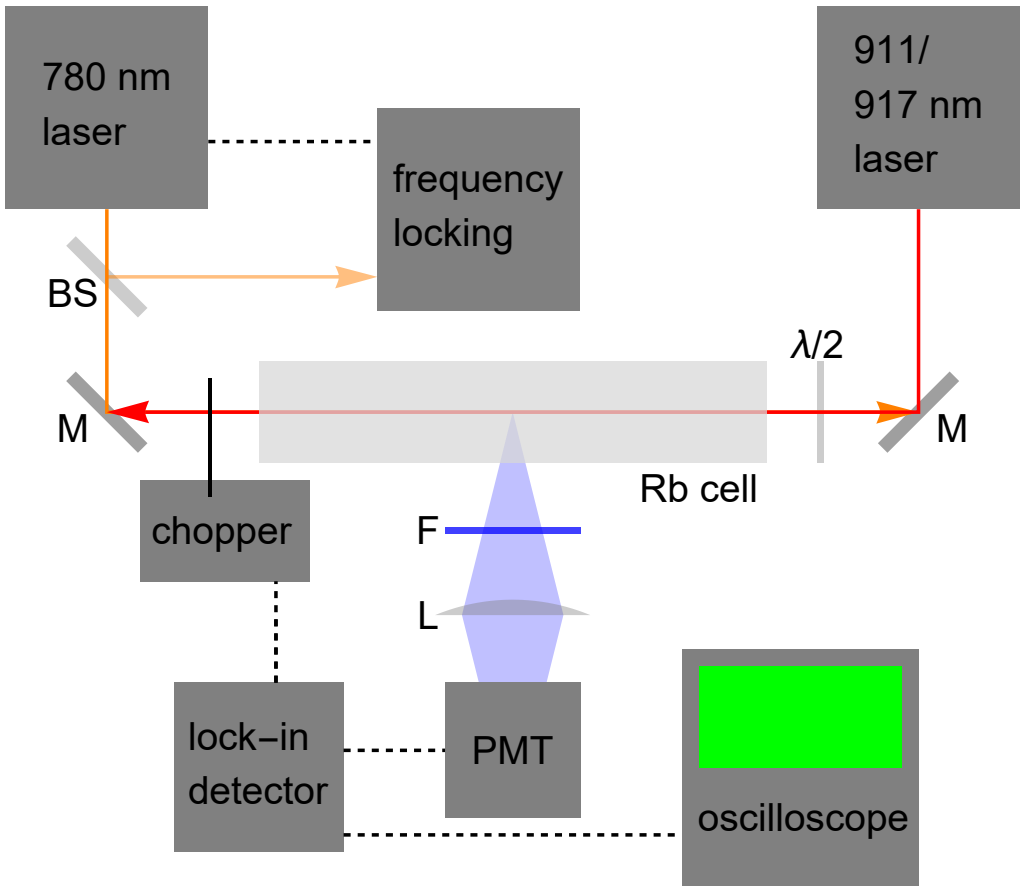

FIG. 1: Experimental setup. F: 420 nm interference filter; L: lens; PMT: photomultiplier tube; M: mirror; BS: beamsplitter; $\lambda/2$ half wave plate used to rotate the linear polarization direction of the 911/917 nm beam.

the hyperfine levels of the $5S$ ground state into states of the hyperfine manifold of the intermediate state $5P_{3/2}$. A second laser (911 or 917 nm) then produces the $5P_{3/2} \rightarrow 6P_J$ ($J = 1/2, 3/2$) forbidden transition. Atoms in the excited $6P_J$ hyperfine states are detected by the emission of a 420 or a 422 nm photon. Through this work we will use the following notation for the hyperfine states involved in the transitions. We use F_1 and M_1 for the $5S$ ground state sublevels, F_2, M_2 for the $5P_{3/2}$ intermediate sublevels, and F_3, M_3 the magnetic sublevels of the $6P_J$ states.

We use the three-step approximation described in our previous papers [29–31], in which the probability for emission of a 420 nm photon is obtained as the product of the populations in the intermediate state $\sigma(F_2, M_2)$ produced by the preparation laser multiplied by the electric quadrupole transition probability and by the electric dipole decay probability from

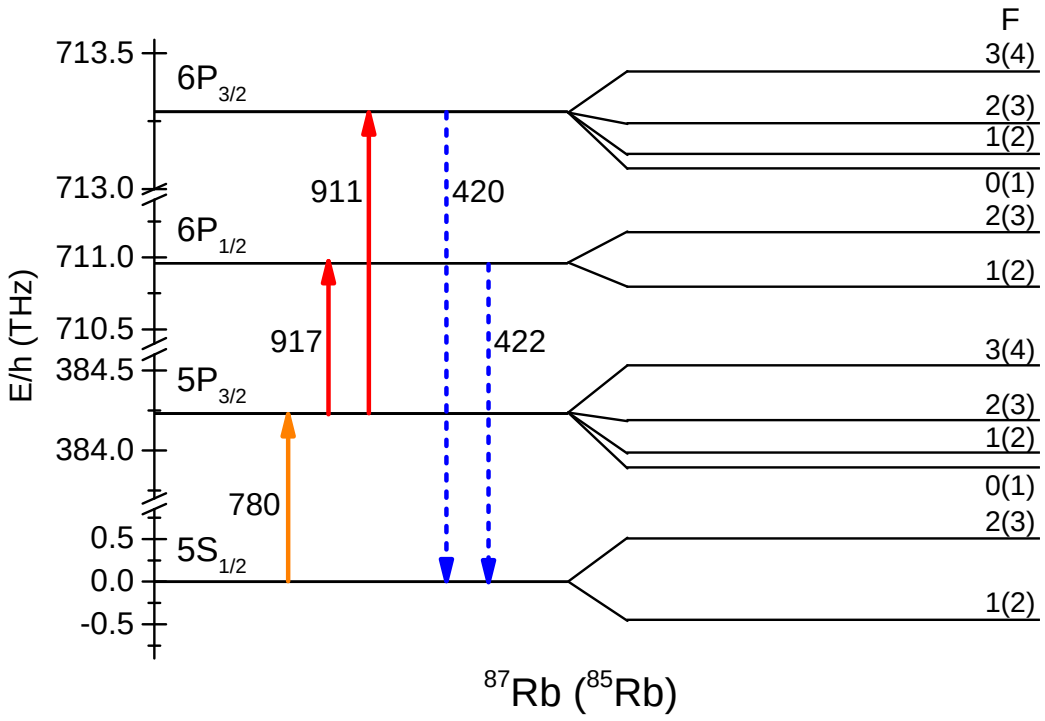

FIG. 2: Energy level diagram for the rubidium atom. The values of the total angular momentum F are indicated in the right hand side of the figure. The hyperfine energy splittings are not drawn with the same scale.

the $6P_J$ state directly into the $5S$ ground state.

For the preparation step one solves the set of rate equations in which the absorption/stimulated emission rates are written as frequency and velocity-dependent terms:

$$B_{ab}\rho(\nu, v) = \frac{r}{\tau_{5P}} \left(\frac{1}{1 + \left[4\pi\tau_{5P}\left(\nu_p - \nu_{ab} - v/\lambda_p\right)\right]^2} \right)$$

Here τ_{5P} is the lifetime of the $5P$ state, ν_p is the frequency of the preparation laser, ν_{ab} is the atomic frequency between states a and b, v is the atom velocity, λ_p is the D2 transition wavelength, and r is the ratio of the preparation laser intensity to the D2 saturation intensity, which is maintained below the Autler-Townes regime [32]. In this expression, the detuning explicitly depends on the atom velocity component along the preparation beam propagation direction. In the rate equations we include decay terms for the spontaneous emission rate

and the loss of atoms because of the transit time $\tau = 1/\gamma$ across a laser beam of finite size:

$$\begin{aligned} \Gamma_a &= \gamma \\ \Gamma_b &= \sum_a A_{ba} + \gamma \end{aligned}$$

Also, we introduce a term that describes the entrance of atoms into the ground state magnetic sublevels with the same rate γ. This allows a steady state solution for all populations that participate in the preparation step.

Figure 3 shows magnetic state populations for the ^{85}Rb $5P_{3/2}F_2M_2$ intermediate state magnetic sublevels when the excitation laser is locked to the $5SF_1 = 3 \rightarrow 5P_{3/2}F_2 = 4$ transition for zero velocity atoms in ^{85}Rb. The figure gives the populations for two values of the laser intensity.

These results indicate that optical pumping produces aligned states with largest populations for $M_F = 0$ at the $F_2 = 2$ and 4 levels, while for $F_2 = 3$ the populations are concentrated in the extreme $M_F = \pm 3$ sublevels. The ordinate scales of the left and right panels in Fig. 3 differ by a factor of two. Therefore, this comparison makes it clear that a factor of two increase in the intensity ratio not only doubles the populations of the magnetic sublevels, but also that the change in intensity also increases the alignment of the three intermediate hyperfine states (for instance, the $M_2 = 0$ bars are larger compared to the other bars in the $F_2 = 4$ and 2 panels). The same factor of two in intensity also reduces the overall contribution of all the $F_2 = 2$ and 3 levels because they can also decay to the $5SF_1 = 2$ dark state. Therefore, the calculation predicts that the relative intensity of the velocity-selection satellite lines decreases as the preparation laser intensity increases. A similar behavior is found for the $5SF_1 = 2 \rightarrow 5P_{3/2}F_2 = 3$ cyclic transition in ^{87}Rb.

The calculation also allows a detailed study of the behavior of the magnetic sublevel populations when the preparation intensity ratio r is varied, and the preparation laser is locked to any frequency of the Doppler broadened profiles. For instance, this is made in Fig. 4. The plot in the left panel gives the populations for the preparation laser frequency locked at the $F_1 = 2 \rightarrow F_2 = 3$ maximum F cyclic transition for zero velocity ^{87}Rb atoms. The plot in the right panel corresponds to the preparation laser locked to the $F_1 = 1 \rightarrow F_2 = 0$ minimum F cyclic transition, also in ^{87}Rb.

All populations show growth rates that saturate for larger values of the intensity ratio r. Even for the largest intensity ratio considered here, the largest population ($M_2 = 0$) is

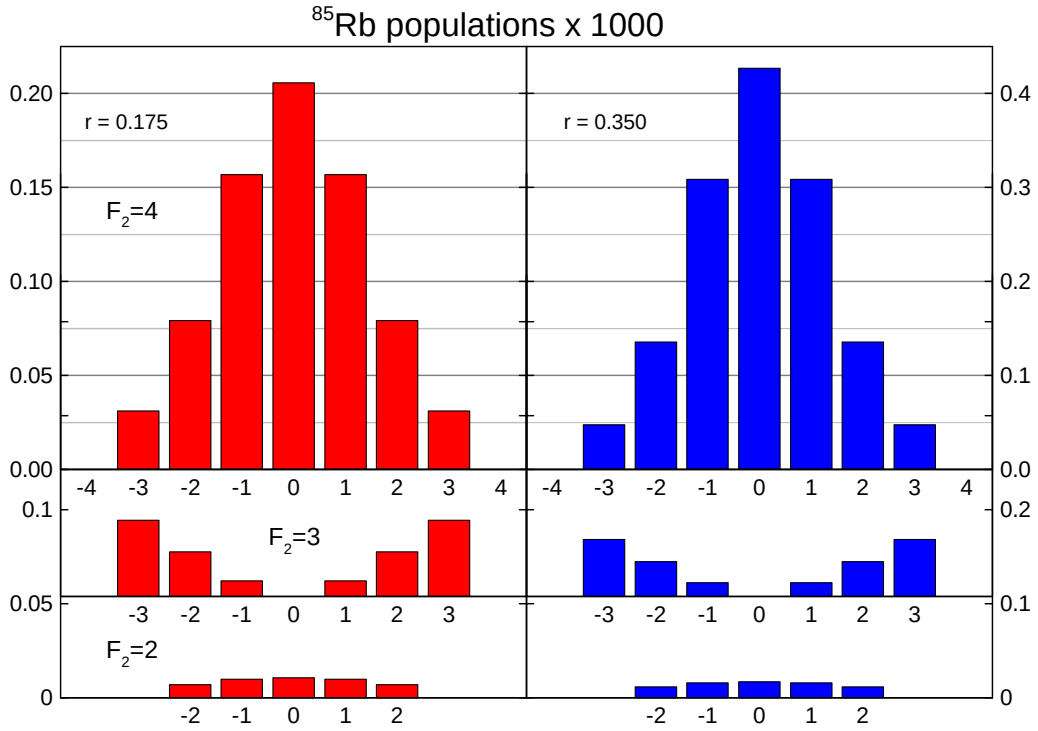

FIG. 3: Populations of the magnetic sublevels of the $5P_{3/2}F_2$ levels in ^{85}Rb for a preparation laser locked to the maximum F transition for zero velocity atoms. The left panel shows the populations obtained with an intensity ratio $r = 0.175$. The right panel gives the populations for $r = 0.350$ and thus the right scale is exactly a factor of 2 times the right scale. All populations were multiplied by a factor of 1000.

less than 0.3% of the total atomic population. When the frequency of the laser is locked to the maximum $F_1 = 2 \rightarrow F_2 = 3$ cyclic transition (left panel) the populations of all magnetic substates of this intermediate state are dominant. Optical pumping effects that deplete the other two hyperfine states ($F_2 = 2$, and 1) are a factor of 30 smaller, and the curves show saturation effects for smaller values of r. The situation is different when the preparation laser is locked to the minimum F cyclic transition $F_1 = 1 \rightarrow F_2 = 0$. Here the dominant populations correspond to $F = 1$, with $M = \pm 1$. In the range of r studied here, the population of $F = 0$ is always lower, but it does not saturate as fast. At the largest value of r considered here, the populations of these two states are almost equal. The populations of the other magnetic substates ($F_2 = 2$ with $M_2 = \pm 2$ and 0) are always smaller, and they

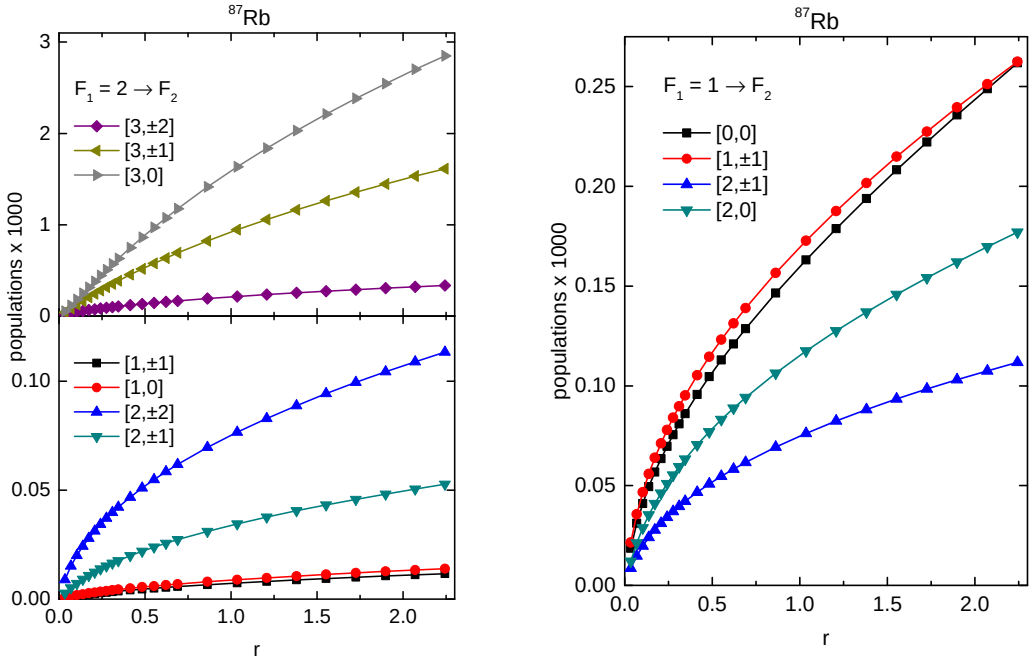

(a) (b)

FIG. 4: ^{87}Rb $5P_{3/2}$ magnetic sublevel populations as functions of the preparation laser intensity ratio r (a) for the $F_1 = 2 \rightarrow F_2$ transitions, and (b) for the $F_1 = 1 \rightarrow F_2$ transitions. The number in square brackets are the values of $[F_2, M_2]$ for each sublevel.

seem to saturate at the same pace as the $F_2 = 1$ $M_2 = \pm 1$ populations. A similar behavior is also found for the sublevel populations of ^{85}Rb. It is important to notice that these relative populations determine the polarization dependence of the electric quadrupole transition into the $6P_J$ states [30, 31].

In the next step, the $5P_{3/2} \rightarrow 6P_j$ electric quadrupole transition probabilities are also written as frequency and velocity-dependent line profiles:

$$P(b,c) = \frac{\sigma_c |\langle b|q|c\rangle|^2}{(\nu_q - \nu_{bc} + v/\lambda_q)^2 + \Gamma_{6P}^2/4)}$$

where ν_q is the frequency of the laser that excites the electric quadrupole transition, $q \propto (e\hat{\epsilon}\cdot\vec{r})(\vec{k}\cdot\vec{r})$ is the electric quadrupole operator, $\hat{\epsilon}$ and $\vec{k}$ are the light polarization and propagation direction. In this expression σ_c represents the population of state c of the $^6P_{3/2}$ hyperfine manifold that results by the electric quadrupole excitation. Here and b and c are, respectively, any of the sublevels of the $5P_{3/2}$ and $6P_J$ hyperfine manifolds, and Γ_{6P} is the

natural width of the $6P$ state. In this expression, the sign of the velocity term indicates that this beam counter-propagates with respect to the preparation beam. The $6P_J \rightarrow 5S$ electric dipole decay probabilities needed for the third step are the same ones used in our previous work [29–31].

One thus obtains an expression for the probability to emit a 420 nm photon that depends on the detuning δ_{ab} of the preparation beam, on the detuning δ_{bc} of the laser that excites the electric quadrupole transition, and on the velocity of the atom. The value of δ_{ab} is fixed to the locked frequency of the preparation laser for each experimental spectrum. The final fluorescence spectrum is the convolution of the resulting function with the atomic velocity distribution function. Finally, to obtain theoretical fluorescence spectra a convolution with a Gaussian (width 5.5 to 9 MHz) is performed to consider instrumental broadening.

IV. RESULTS AND DISCUSSION.

In our previous results [29–31] it was shown that the use of the static population equations for the preparation step allowed a direct calculation of the relative populations of the $5SF_1 = I + 1/2 \rightarrow 5P_{3/2}F_2 = I + 3/2$ cyclic transition in both isotopes. Furthermore, when these intermediate state populations are combined with the polarization states of the radiation used to produced the electric quadrupole excitation, strongly anisotropic fluorescence spectra are obtained. Here we show that the calculation that includes the velocity dependent populations in the preparation step not only reproduces the previous results, but it also gives a rather accurate description of the behavior of the electric quadrupole transition satellites. One example of this can be found in Fig. 5, which shows the comparison of fluorescence emission obtained with parallel and perpendicular linear polarizations of the preparation and the electric quadrupole transition radiation for ^{87}Rb. These spectra were recorded for an intensity ratio of $r = 0.31$, which is significantly below saturation. In this figure the first number of each parenthesis is the value of F_2 in the $5P_{3/2}$ intermediate hyperfine state, and the second number gives the value of F_3 in the $6P_J$ state after the quadrupole transition. The spectra in Fig. 5 are dominated by the lines produced by an electric quadrupole excitation from the $F_2 = 3$ state. However, three satellites can be observed, especially for perpendicular polarizations. These satellites originate from the $F_2 = 2$ intermediate state which is produced by selection of velocities in the Doppler-broadened gas. In both polarization

configurations the positions and relative contributions of these satellites are well reproduced by the velocity dependent calculation. It is important to point out the complete absence of the $F_2 = 2 \rightarrow F_3 = 2$ line, which corresponds to an electric quadrupole forbidden transition.

A similar comparison is made for fluorescence emission that follows the preparation and electric quadrupole excitation of ^{85}Rb atoms. The spectra recorded with parallel and perpendicular polarizations are shown in Fig. 6. In this case, the intensity ratio of the preparation step is $r = 1.55$, significantly larger than the previous case. These spectra are dominated by the electric quadrupole transitions originating from the $5P_{3/2}F_2 = 4$ state. Once again, the relative intensities are determined by the relative polarizations of the two lasers. The calculation reproduces well the relative intensities, and it also predicts the presence of two satellite peaks at the high end of each spectrum. However, the calculation overestimates the contribution of the Lorentzian wings both between the $(4, 3)$ and $(4, 4)$ peaks, and in the region of the $(3, 4)$ and $(2, 4)$ satellites. It will be shown later that this strong reduction of the velocity selection satellites occurs because of optical pumping effects that reduce the populations of the $5P_{3/2}F_2 = 3$ and 4 states.

This analysis also includes the emission spectra that follows the $5P_{3/2} \rightarrow 6P_{1/2}$ electric quadrupole excitation first reported in [31]. The spectra for this second fine structure component of ^{85}Rb are presented in Fig. 7. Once again, spectra with parallel and perpendicular polarizations are given, and the comparison with the calculation is made in both cases. The two spectra are dominated by the $(4, 2)$ and $(4, 3)$ electric quadrupole excitations for zero velocity atoms, but there are also clear indications of the other satellite lines. Again, their relative contribution is stronger for the perpendicular polarization configuration, something that is in very good agreement with the calculation. A major difference is now that there are significant contributions from the three ($F_2 = 4$, 3 and 2) intermediate hyperfine states in both $F_3 = 2$ and 3 manifolds. The comparison also shows that the theory overestimates the contribution from the wings at the high energy side of each manifold.

We now present the behavior of the satellite lines as a function of the intensity of the preparation step. Figure 8 compares three spectra for ^{85}Rb recorded with parallel polarizations and different values of the preparation light intensity. The spectra are dominated by the $5P_{3/2}F_2 = 4 \rightarrow 6P_{3/2}F_3$ electric quadrupole transitions for zero velocity atoms. For the lowest intensity the two high-frequency satellites are very well defined, but as the preparation

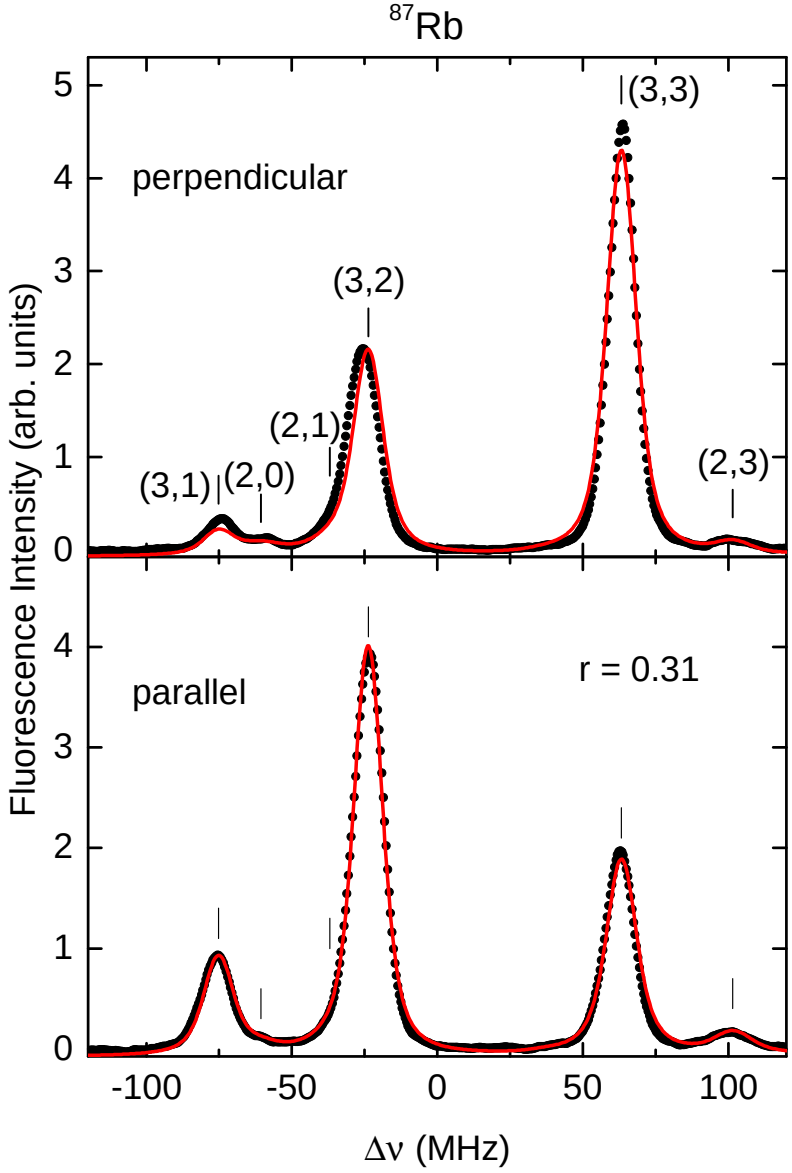

FIG. 5: Comparison between experimental spectra and the results of a rate equation calculation for the $5P_{3/2} \rightarrow 6P_{3/2}$ transition in ^{87}Rb. Top spectrum: perpendicular linear polarizations of preparation and quadrupole laser beams. Bottom spectrum: parallel linear polarizations. The position of the expected resonances is indicated by vertical lines. The numbers in parenthesis indicate the values of F_2 and F_3 for each transition. The black dots correspond to the experimental spectra and the continuous red lines give the results of the calculation.

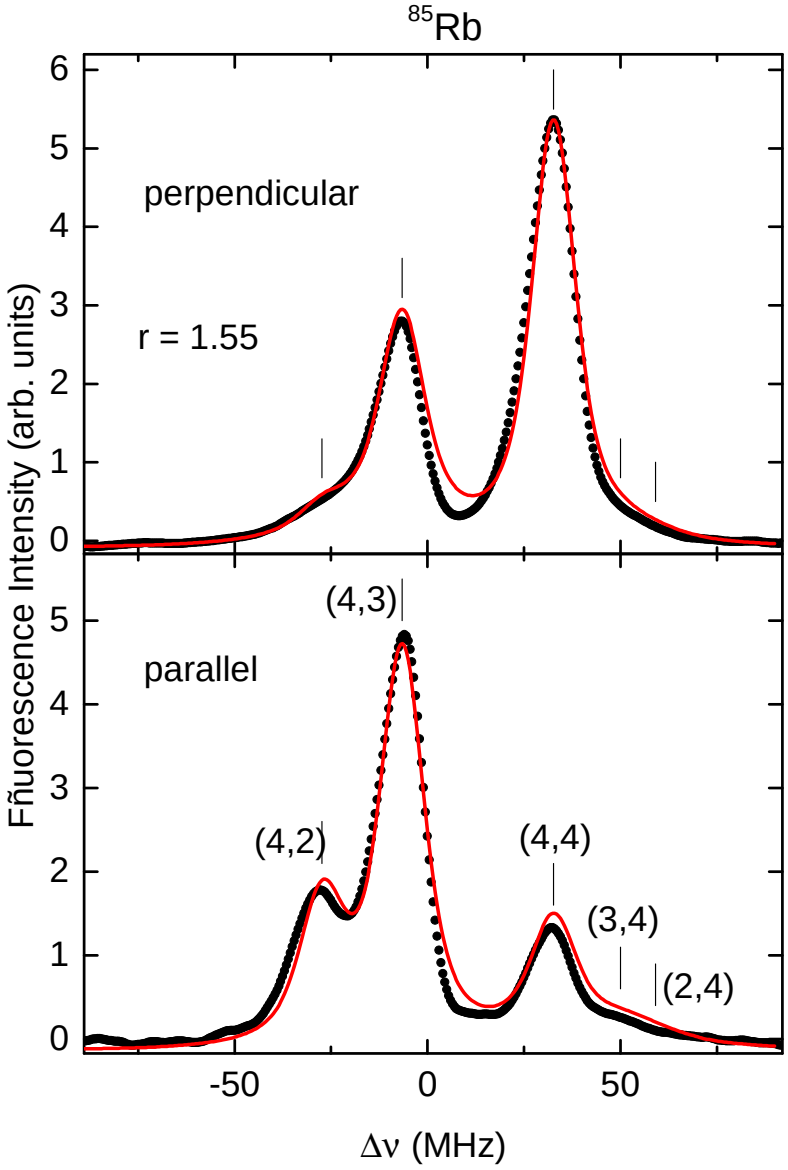

FIG. 6: Comparison between experimental spectra and the results of a rate equation calculation for the $5P_{3/2} \rightarrow 6P_{3/2}$ transition in ^{85}Rb. Top spectrum: perpendicular linear polarizations of preparation and quadrupole laser beams. Bottom spectrum: parallel linear polarizations. The position of the expected resonances is indicated by vertical lines. The numbers in parenthesis indicate the values of F_2 and F_3 for each transition.

intensity is increased their relative contribution is reduced. For the top spectrum (and in

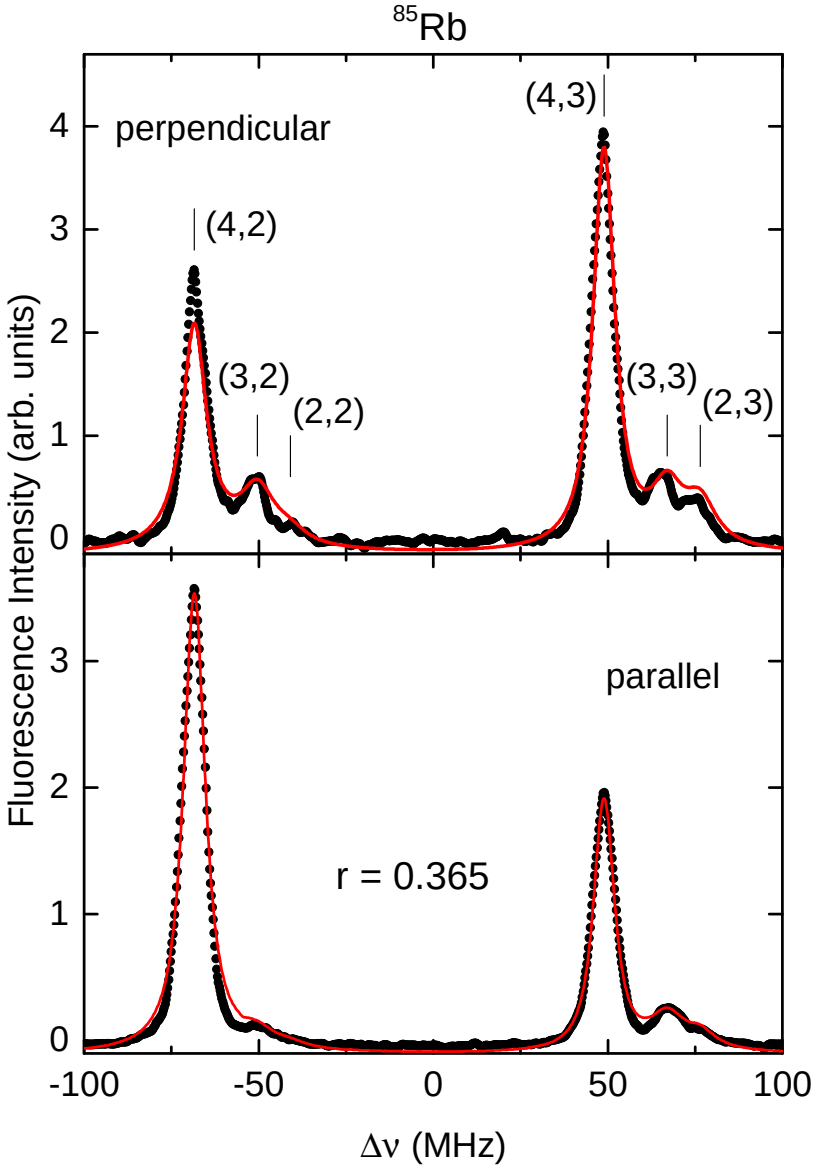

FIG. 7: Comparison between esperimental spectra and the results of a rate equation calculation for the $5P_{3/2} \rightarrow 6P_{1/2}$ transition in ^{85}Rb. Top spectrum: perpendicular linear polarizations of preparation and quadrupole laser beams. Bottom spectrum: parallel linear polarizations. The position of the expected resonances is indicated by vertical lines. The numbers in parenthesis indicate the values of F_2 and F_3 for each transition.

the equivalent spectra of Fig. 8) the satellites are barely discernible from the high-frequency

Lorentzian wing. These results are in agreement with the calculation, that predicts a steady reduction in the satellite contribution because the preparation step pumps population out of the $5P_{3/2}F_2 = 2$ and 1 hyperfine states that are produced by non-cyclic transitions and for non-zero velocities.

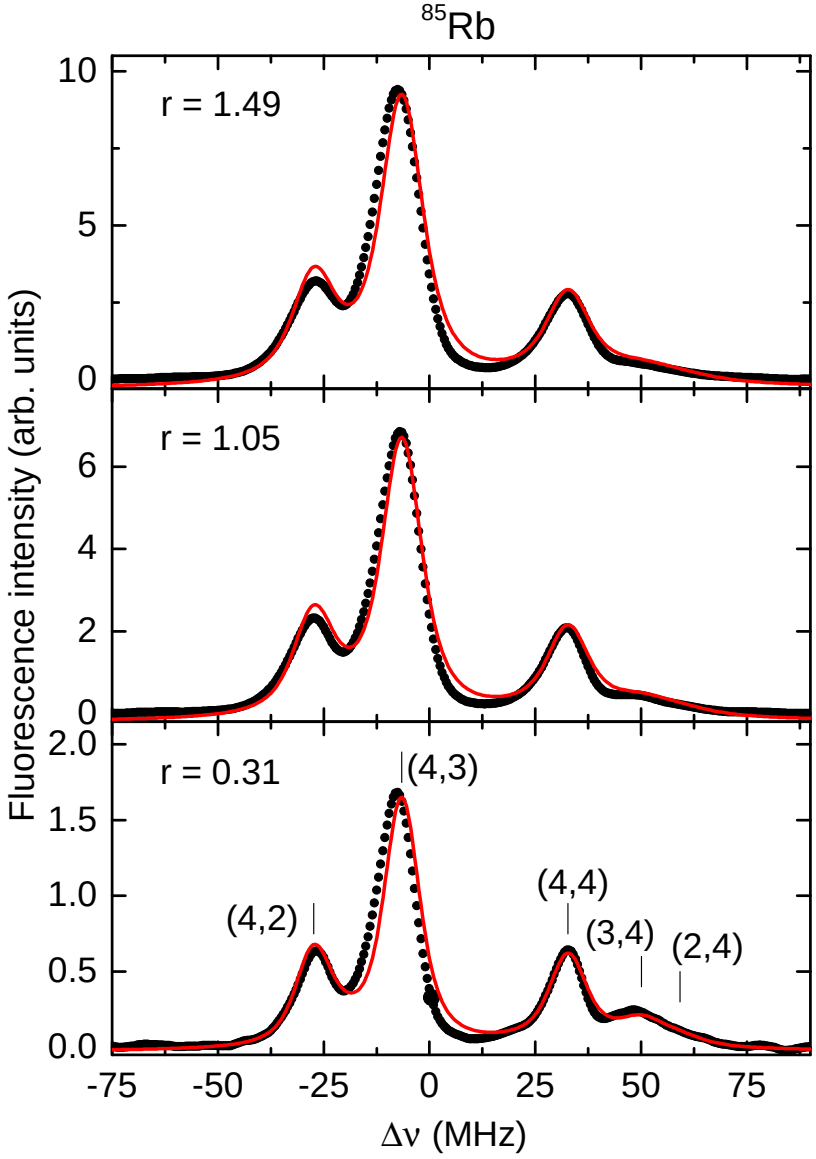

FIG. 8: Spectra of the $5P_{3/2} \rightarrow 6P_{3/2}$ forbidden transition recorded at three values of the preparation laser intensity r.

A similar reduction of the relative satellite contribution was found for the spectra of ^{87}Rb. Three examples of this effect are given in Fig. 9. The three satellites are clearly present in the bottom spectrum recorded at the lowest intensity. In this case, it is even tempting to assign what appears to be a peak at 37.0 MHz to the $(1, 2)$ electric quadrupole transition. However, in this case this bump is at the same level as the background. The relative contribution of the three identified satellites diminishes as the intensity of the preparation laser is increased. This is in agreement with the result of the calculation, and it results from a reduction of the relative $5P_{3/2}F_2 = 2$ populations prepared with a non-cyclic transition.

Finally, we present for the first time results for the fluorescence in ^{87}Rb that follows the $5SF_1 = 1 \rightarrow 5P_{3/2}F_2 = 0$, 1 and 2 preparation and the electric quadrupole excitation. One would expect that for this minimum F cyclic preparation transition the fluorescence spectra should be dominated by electric quadrupole excitations from the $F_2 = 0$ intermediate hyperfine state. Furthermore, the electric quadrupole selection rules prevent transitions to the $F_3 = 0$ and 1 states. Therefore, one would expect a strong single fluorescence peak. However, the calculation predicts that optical pumping and velocity selection effects in the preparation step (see Fig. 4b) produce significant populations in other intermediate hyperfine states for nonzero velocities. The experimental fluorescence spectrum obtained for this preparation is shown in Fig. 10. In this case, the signal to background is low, and this spectrum actually is the average of more than 30 individual spectra. The spectrum is composed of three independent groups, with a central dominant line that would appear to result from a single electric quadrupole transition. However, the calculation (red line) indicates the presence of seven electric quadrupole transitions that start in different $5P_{3/2}$ hyperfine states prepared at different velocities. Once again, the electric quadrupole selection rules do not allow the $F_2 = 2 \rightarrow F_3 = 2$ transition. According to this calculation, there are two transitions that contribute to the strongest, central line. Both transitions originate from the states with the highest populations in the intermediate state, namely $F_2 = 0$ and 1 (see Fig. 4b). To test the overall prediction of the calculation, a set of seven Voigt peaks of equal widths were fit to the data. The result of this fit gives the emission lines at the positions given by the calculation, but with relative intensities that are not in agreement. In particular, the experiment shows either a reduction of the electric quadrupole transitions that start in the $F_2 = 2$ hyperfine state, or an increase in the transitions originating in the $F_2 = 1$ intermediate state. It is important to point out that such an increase in the electric

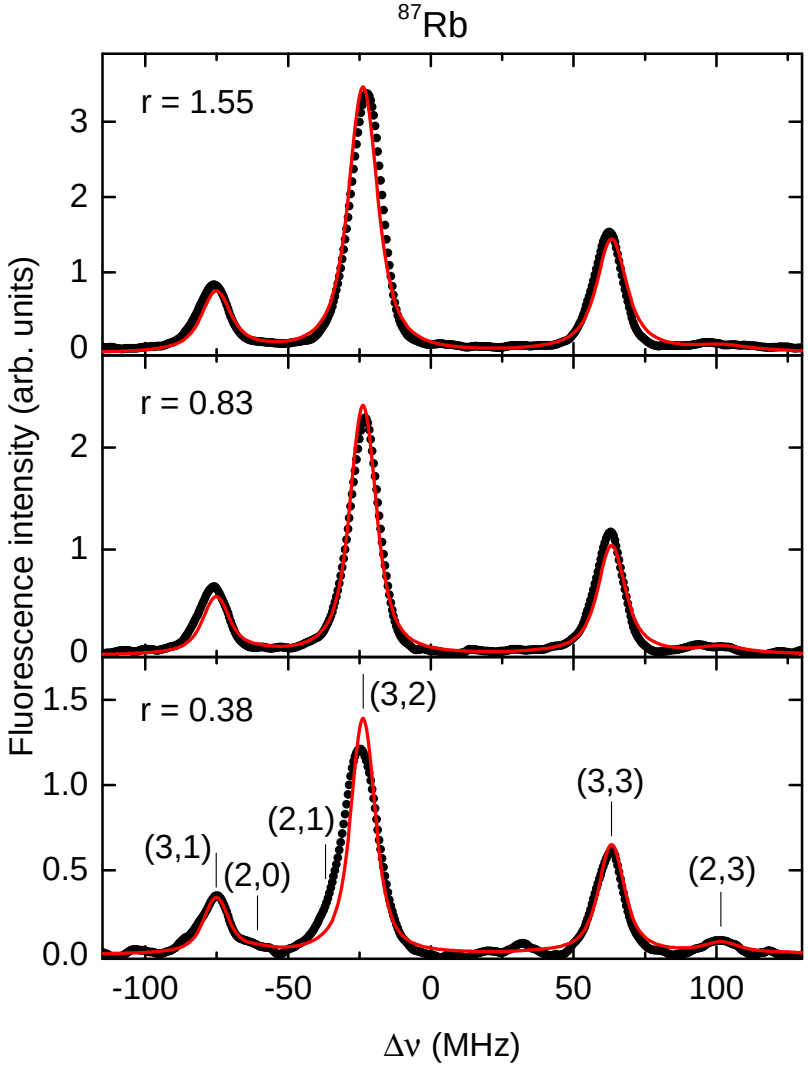

FIG. 9: Spectra of the $5P_{3/2} \rightarrow 6P_{3/2}$ forbidden transition in ^{87}Rb recorded at three values of the preparation laser intensity r.

quadrupole intensity from the $F_2 = 1$ state seems to occur for $\Delta F = 0$, 1, and 2. The latter is allowed by an electric quadrupole transition only. Therefore, the discrepancy between theory and experiment cannot be assigned to the presence of magnetic dipole transitions.

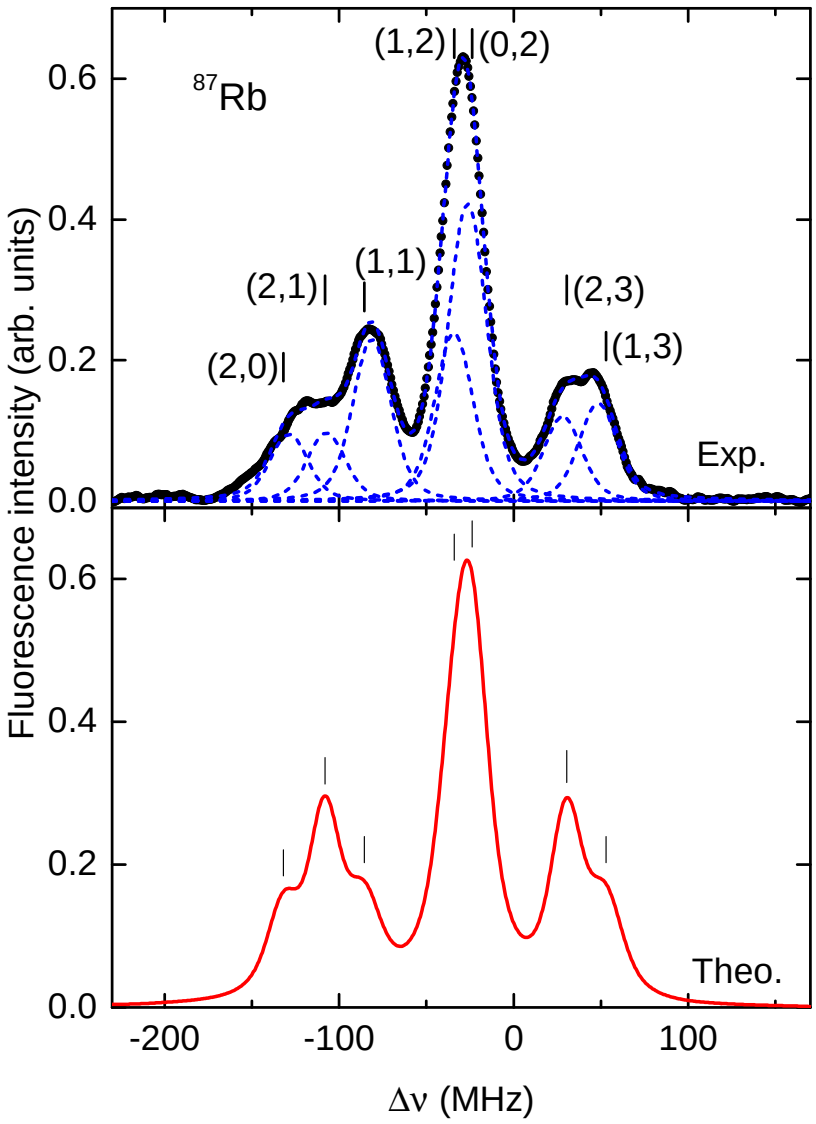

FIG. 10: Comparison between experiment and theory for the $5P_{3/2} \rightarrow 6P_{3/2}$ transition starting in the $F = 1$ manifold of the $5S$ initial state.

V. CONCLUSIONS.

The results presented in this work provide a deeper understanding $5P_{3/2} \rightarrow 6P_J$ electric quadrupole transition in atomic rubidium. It is shown that the strong difference in transition probabilities between the preparation (electric dipole) and the electric quadrupole step allows

an extension of the three-step model presented in references [29, 30] to include selection of velocity effects. When these effects are included in the rate equations, one can calculate fluorescence spectra that include satellite lines and are in very good agreement with the experiment for electric quadrupole transitions into both $6P_J$ fine structure states. Light polarization effects are also present in the velocity-selected satellite lines, but they are not as strong as with the main electric quadrupole lines. This results in larger relative intensities when the polarization of the electric quadrupole step is perpendicular to the polarization of the preparation step. Experiment and theory also agree in showing a reduction of the relative contribution of the velocity-selected satellites as the intensity of the preparation laser is increased. The dynamic rate equation calculation was shown to be necessary to interpret the fluorescence spectra obtained with the preparation laser locked at minimum F cyclic transition of the preparation step. In this case selection of velocity effects resulted in the production of seven distinct fluorescence lines. These experiments show that the observed forbidden excitations are the result of electric quadrupole transitions, with no indication of any contribution from magnetic dipole transitions.

ACKNOWLEDGMENTS

We thank J. Rangel for his help in the construction of the diode laser. This work was supported by DGAPA-UNAM, México, under projects PAPIIT Nos. IN114719 and IN117120; and by Consejo Nacional de Ciencia y Tecnología (CONACyT) and CTIC-UNAM via the Basic Science Grant SEP-CONACyT project No. 285289, and the National Laboratories Program, Grants No. 280181, No. 293471, and No. 299057. L.M. Hoyos-Campo thanks UNAM-DGAPA and Conacyt for the postdoctoral fellowship.

[1] V. K. Dubrovich and S. I. Grachev, Recombination dynamics of primordial hydrogen and helium (HeI) in the universe, Astron. Lett. **31**, 359 (2005).

[2] M.-A. Bouchiat and C. Bouchiat, Parity violation in atoms, Rep. Prog. Phys **60**, 1351 (1997).

[3] B. M. Roberts, V. A. Dzuba, and V. V. Flambaum, Nuclear-spin-dependent parity nonconservation in $s - d_{5/2}$ and $s - d_{3/2}$ transitions, Phys Rev A **89**, 012502 (2014).

[4] J. Preskill, Reliable quantum computers, Proceedings of the Royal Society A **454**, 385 (1998).

[5] C. Langer, R. Ozeri, J. D. Jost, J. Chiaverini, B. Demarco, A. Ben-Kish, R. B. Blakestad, J. Britton, D. B. Hume, W. M. Itano, D. Leibfried, R. Reichle, T. Rosenband, T. Schaetz, P. O. Schmidt, and D. J. Wineland, Long-lived qubit memory using atomic ions, Phys Rev Lett **95**, 060502 (2005).

[6] A. V. Taichenachev, V. I. Yudin, C. W. Oates, C. W. Hoyt, Z. W. Barber, and L. Hollberg, Magnetic field-induced spectroscopy of forbidden optical transitions with application to lattice-based optical atomic clocks, Phys Rev Lett **96**, 083001 (2006).

[7] A. D. Ludlow, M. M. Boyd, J. Ye, E. Peik, and P. O. Schmidt, Optical atomic clocks, Rev Mod Phys **87**, 637 (2015).

[8] F. W. Knollmann, A. N. Patel, and S. C. Doret, Part-per-billion measurement of the $4^2S_{1/2} \rightarrow 3^2D_{5/2}$ electric-quadrupole-transition isotope shifts between $^{42,44,48}Ca^+$ and $^{40}Ca^+$, Phys Rev A **100**, 022514 (2019).

[9] I. Counts, J. Hur, D. P. A. Craik, H. Jeon, C. Leung, J. C. Berengut, A. Geddes, A. Kawasaki, W. Jhe, and V. Vuletić, Evidence for nonlinear isotope shift in Yb^+ search for new boson, Phys Rev Lett **125**, 123002 (2020).

[10] S. Tojo, M. Hasuo, and T. Fujimoto, Absorption Enhancement of an Electric Quadrupole Transition of Cesium Atoms in an Evanescent Field, Phys Rev Lett **92**, 053001 (2004).

[11] S. Tojo, T. Fujimoto, and M. Hasuo, Precision measurement of the oscillator strength of the cesium $6^2S_{1/2} \rightarrow 5^2D_{5/2}$ electric quadrupole transition in propagating and evanescent wave fields, Phys Rev A **71**, 012507 (2005).

[12] F. Le Kien, T. Ray, T. Nieddu, T. Busch, and S. Nic Chormaic, Enhancement of the quadrupole interaction of an atom with the guided light of an ultrathin optical fiber, Phys. Rev. A **97**, 013821 (2018), arXiv:1709.06700.

[13] T. Ray, R. K. Gupta, V. Gokhroo, J. L. Everett, T. Nieddu, K. S. Rajasree, and S. N. Chormaic, Observation of the ^{87}Rb $5S_{1/2} \rightarrow 4D_{3/2}$ electric quadrupole transition at 516.6 nm mediated via an optical nanofibre, New J Phys **22**, 062001 (2020).

[14] V. E. Lembessis and M. Babiker, Enhanced quadrupole effects for atoms in optical vortices, Phys Rev Lett **110**, 083002 (2013).

[15] K. Sakai, T. Yamamoto, and K. Sasaki, Nanofocusing of structured light for quadrupolar light-matter interactions, Sci. Rep. **8**, 7746 (2018).

[16] G. Hakhumyan, C. Leroy, R. Mirzoyan, Y. Pashayan-Leroy, and D. Sarkisyan, Study of "forbidden" atomic transitions on D2 line using Rb nano-cell placed in external magnetic field, Eur Phys J D **66**, 119 (2012).

[17] A. Sargsyan, A. Tonoyan, G. Hakhumyan, A. Papoyan, E. Mariotti, and D. Sarkisyan, Giant modification of atomic transition probabilities induced by a magnetic field: forbidden transitions become predominant, Laser Phys Lett **11**, 055701 (2014).

[18] K. Shibata, S. Tojo, and D. Bloch, Excitation enhancement in electric multipole transitions near a nanoedge, Opt Express **25**, 9476 (2017).

[19] E. A. Chan, S. A. Aljunid, G. Adamo, N. I. Zheludev, M. Ducloy, and D. Wilkowski, Coupling of atomic quadrupole transitions with resonant surface plasmons, Phys. Rev. A **99**, 063801 (2019).

[20] K. Sakai, H. Kitajima, and K. Sasaki, Plasmonic nanostructures for shrinking structured light to access forbidden transitions, Nanophotonics **11**, 2465 (2022).

[21] R. Gutiérrez-Jáuregui and R. Jáuregui, Nonlinear Quantum Optics With Structured Light: Tightly Trapped Atoms in the 3D Focus of Vectorial Waves, Front. Phys. **10**, 10.3389/fphy.2022.896174 (2022).

[22] R. J. Rafac, B. C. Young, J. A. Beall, W. M. Itano, D. J. Wineland, and J. C. Bergquist, Sub-dekahertz Ultraviolet Spectroscopy of $^{199}Hg^{+}$, Phys Rev Lett **85**, 2462 (2000).

[23] M. Bhattacharya, C. Haimberger, and N. Bigelow, Forbidden Transitions in a Magneto-Optical Trap, Phys Rev Lett **91**, 213004 (2003).

[24] R. Pires, M. Ascoli, E. E. Eyler, and P. L. Gould, Upper limit on the magnetic dipole contribution to the $5p - 8p$ transition in Rb by use of ultracold atom spectroscopy, Phys Rev A **80**, 062502 (2009).

[25] D. Tong, S. Farooqi, E. van Kempen, Z. Pavlovic, J. Stanojevic, R. Côté, E. Eyler, and P. Gould, Observation of electric quadrupole transitions to Rydberg nd states of ultracold rubidium atoms, Phys Rev A **79**, 052509 (2009).

[26] E. A. Chan, S. A. Aljunid, N. I. Zheludev, D. Wilkowski, and M. Ducloy, Doppler-free approach to optical pumping dynamics in the $6S_{1/2} \rightarrow 5D_{5/2}$ electric quadrupole transition of cesium vapor, Opt Lett **41**, 2005 (2016).

[27] S. Pucher, Spectroscopy of the $6S_{1/2} \rightarrow 5D_{5/2}$ Electric Quadrupole Transition of Atomic Cesium, Master's Thesis, Technischen Universität, Wien, Austria (2018).

[28] S. B. Bayram, M. D. Havey, D. V. Kupriyanov, and I. M. Sokolov, Anomalous depolarization of the $5p^2P_{3/2} \rightarrow 8p^2P_{j'}$ transitions in atomic ^{87}Rb, Phys Rev A **62**, 12503 (2000).

[29] F. Ponciano-Ojeda, S. Hernández-Gómez, O. López-Hernández, C. Mojica-Casique, R. Colín-Rodríguez, F. Ramírez-Martínez, J. Flores-Mijangos, D. Sahagún, R. Jáuregui, and J. Jiménez-Mier, Observation of the $5p_{3/2} \rightarrow 6p_{3/2}$ electric-dipole-forbidden transition in atomic rubidium using optical-optical double-resonance spectroscopy, Phys. Rev. A **92**, 42511 (2015).

[30] C. Mojica-Casique, F. Ponciano-Ojeda, S. Hernández-Gómez, O. López-Hernández, J. Flores-Mijangos, F. Ramírez-Martínez, D. Sahagún, R. Jáuregui, and J. Jiménez-Mier, Control of electronic magnetic state population via light polarization in the $5p_{3/2} \rightarrow 6p_{3/2}$ electric quadrupole transition in atomic rubidium, J. Phys. B **20**, 025003 (2017).

[31] F. Ponciano-Ojeda, C. Mojica-Casique, S. Hernández-Gómez, O. López-Hernández, L. Hoyos-Campo, J. Flores-Mijangos, F. Ramírez-Martínez, D. Sahagún, R. Jáuregui, and J. Jiménez-Mier, Optical spectroscopy of the $5p_{3/2} \rightarrow 6p_{1/2}$ electric dipole-forbidden transition in atomic rubidium, J. Phys. B **52**, 135001 (2019).

[32] F. Ramírez-Martínez, F. Ponciano-Ojeda, S. Hernández-Gómez, A. D. Angel, C. Mojica-Casique, L. M. Hoyos-Campo, J. Flores-Mijangos, D. Sahagún, R. Jáuregui, and J. Jiménez-Mier, Electric-dipole forbidden transitions for probing atomic state preparation: The case of the Autler-Townes effect, J. Phys. B **54**, 095002 (2021).

[33] D. Main, T. M. Hird, S. Gao, I. A. Walmsley, and P. M. Ledingham, Room temperature atomic frequency comb storage for light, Opt Lett **46**, 2960 (2021).

[34] D. Main, T. M. Hird, S. Gao, E. Oguz, D. J. Saunders, I. A. Walmsley, and P. M. Ledingham, Preparing narrow velocity distributions for quantum memories in room-temperature alkali-metal vapors, Phys. Rev. A **103**, 043105 (2021).

[35] A. Aspect, E. Arimondo, R. Kaiser, N. Vansteenkiste, and C. Cohen-Tannoudji, Laser cooling below the one-photon recoil energy by velocity-selective coherent population trapping, Phys. Rev. Lett. **61**, 826 (1988).

[36] H. G. Lee, S. Park, M. H. Seo, and D. Cho, Motion-selective coherent population trapping for subrecoil cooling of optically trapped atoms outside the Lamb-Dicke regime, Phys. Rev. A **106**, 023324 (2022).

[37] S. Park, M. H. Seo, R. A. Kim, and D. Cho, Motion-selective coherent population trapping by Raman sideband cooling along two paths in a Λ configuration, Phys. Rev. A **106**, 023323 (2022).

[38] E. Talker, P. Arora, Y. Barash, D. Wilkowski, and U. Levy, Efficient optical pumping of alkaline atoms for evanescent fields at dielectric-vapor interfaces, Opt. Express **27**, 33445 (2019).

[39] E. Talker, P. Arora, Y. Barash, L. Stern, and U. Levy, Plasmonic enhanced EIT and velocity selective optical pumping measurements with atomic vapor, ACS Photonics **5**, 2609 (2018).

[40] L. D. Turner, V. Karaganov, P. J. O. Teubner, and R. E. Scholten, Sub-Doppler bandwidth atomic optical filter, Opt Lett **27**, 500 (2002).

[41] A. Cerè, V. Parigi, M. Abad, F. Wolfgramm, A. Predojević, and M. W. Mitchell, Narrowband tunable filter based on velocity-selective optical pumping in an atomic vapor, Opt Lett **34**, 1012 (2009).

[42] X. H. Bao, Y. Qian, J. Yang, H. Zhang, Z. B. Chen, T. Yang, and J. W. Pan, Generation of narrow-band polarization-entangled photon pairs for atomic quantum memories, Phys. Rev. Lett. **101**, 190501 (2008).

[43] G. Wang, Y. S. Wang, E. K. Huang, W. Hung, K. L. Chao, P. Y. Wu, Y. H. Chen, and I. A. Yu, Ultranarrow-bandwidth filter based on a thermal EIT medium, Sci. Rep. **8**, 7959 (2018).

Figure 1

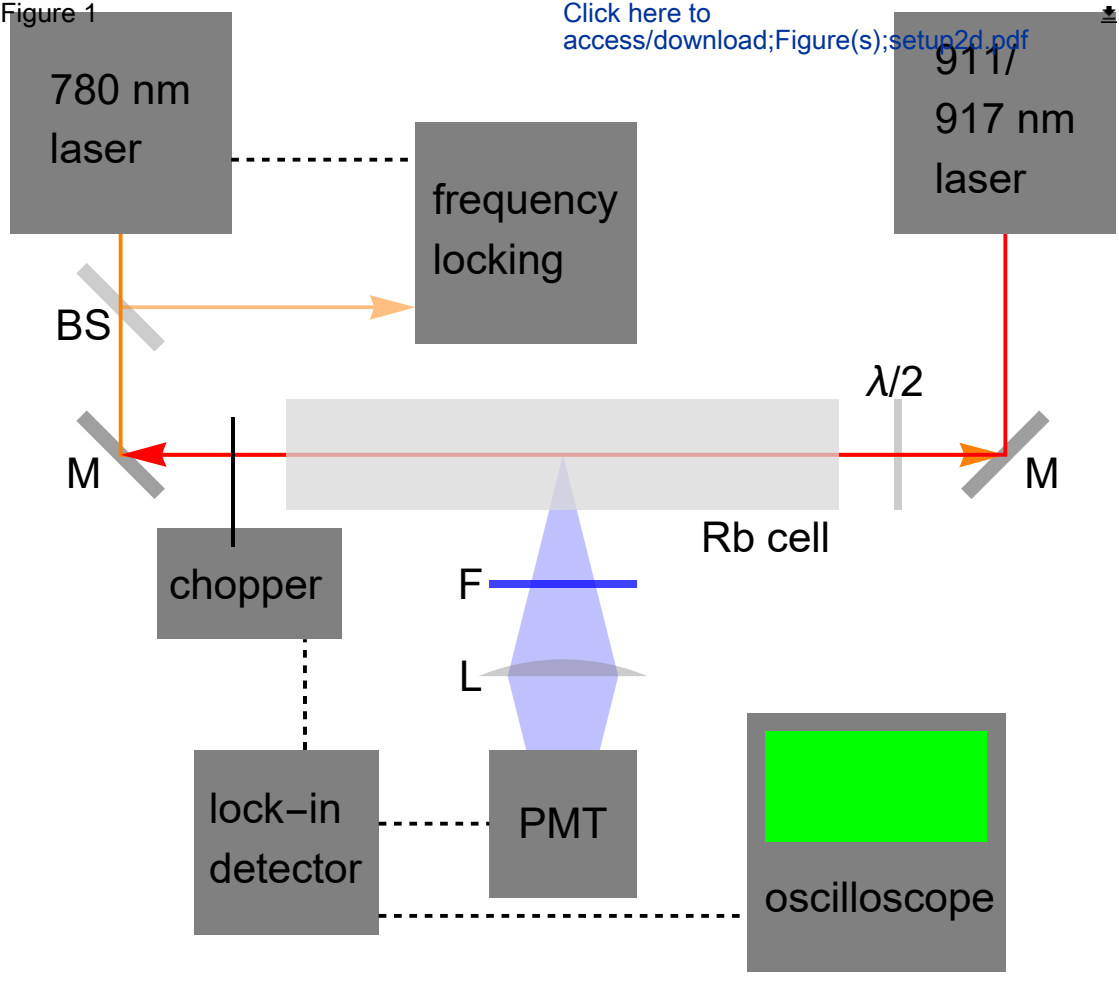

Figure 2

Click here to access/download;Figure(s);Rb8587EnLvl.pdf

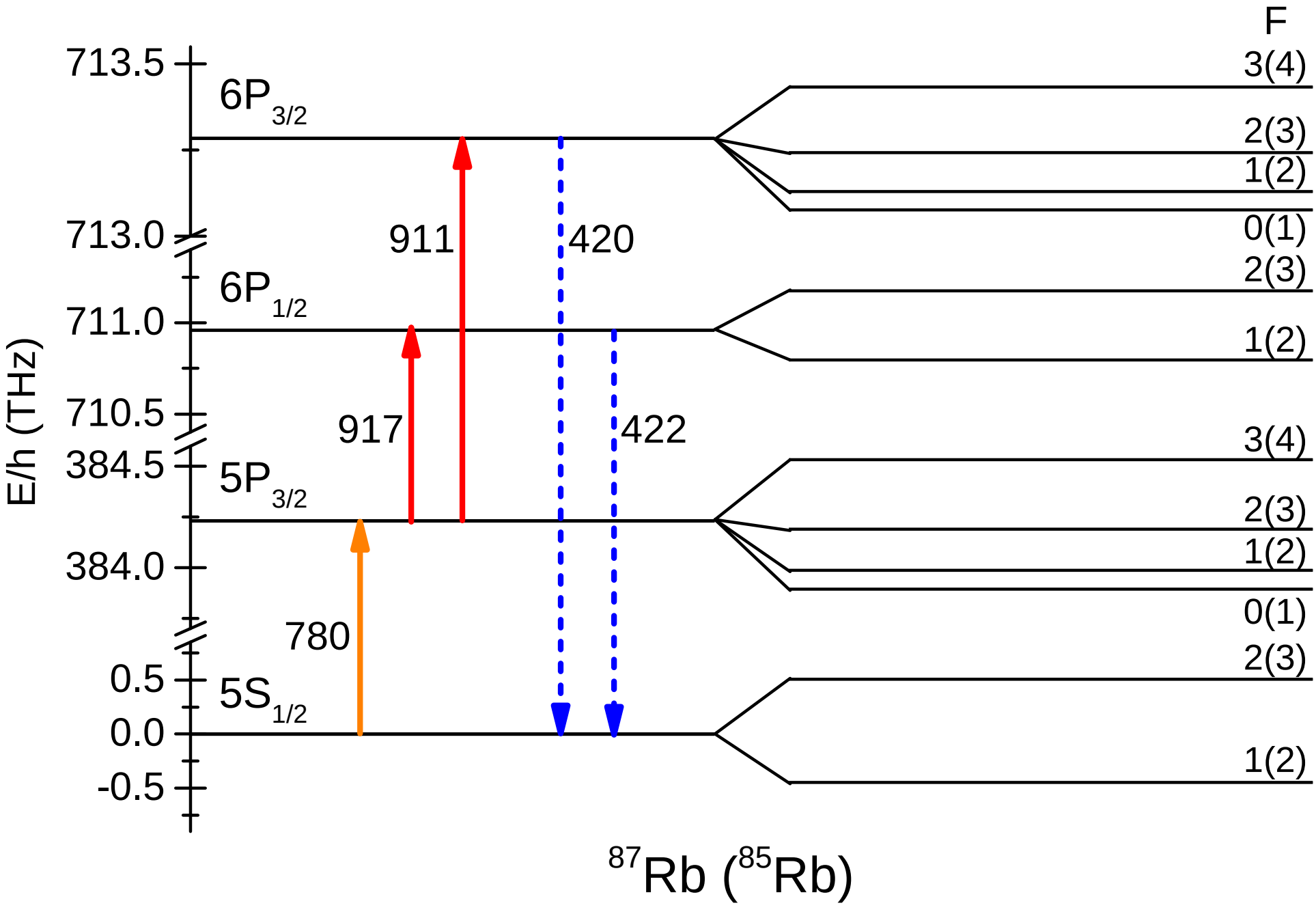

Figure 3

Click here to access/download;Figure(s);Populations85Rb.pdf

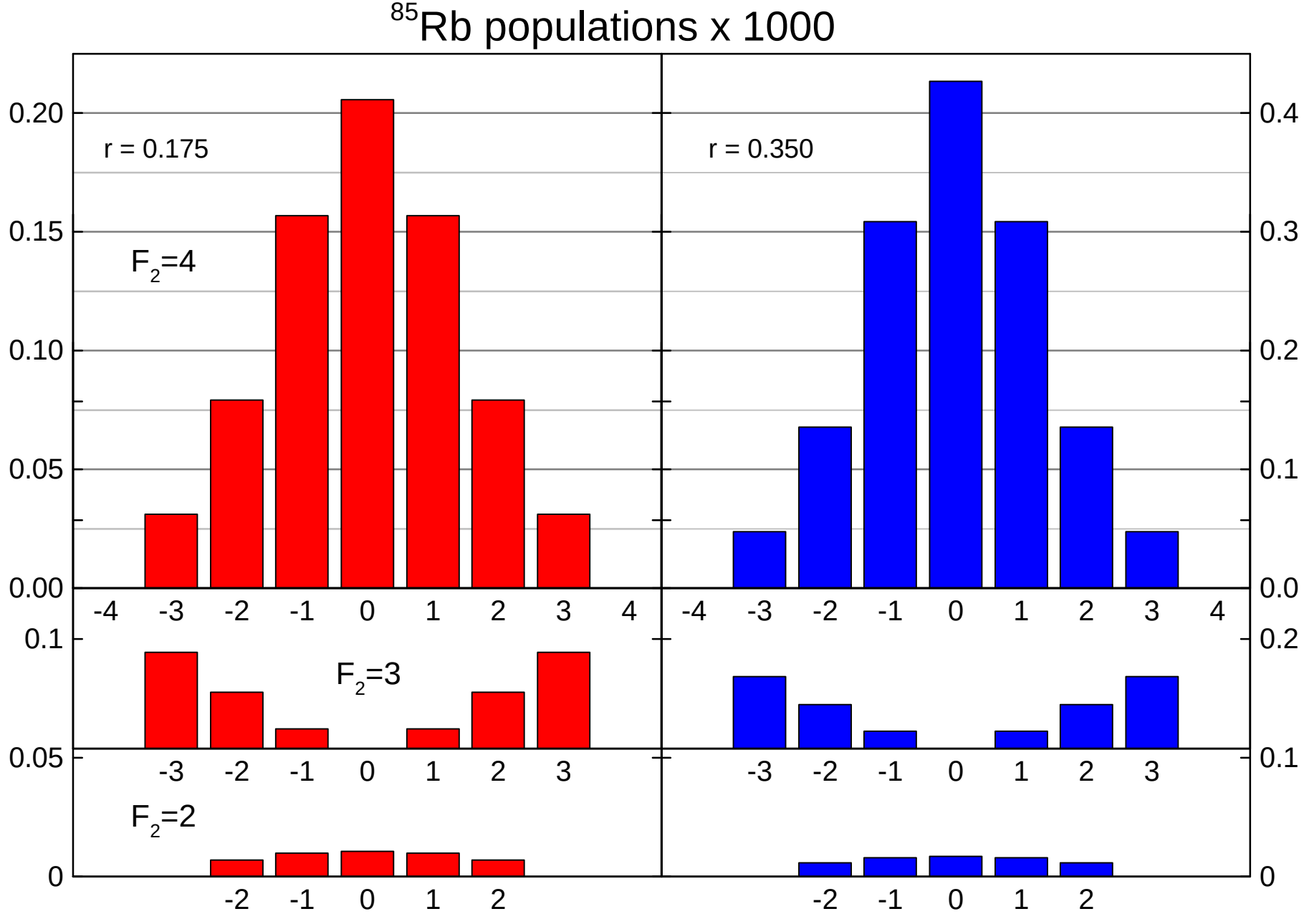

Figure4a

Click here to access/download;Figure(s);Rb87populationsH.pdf

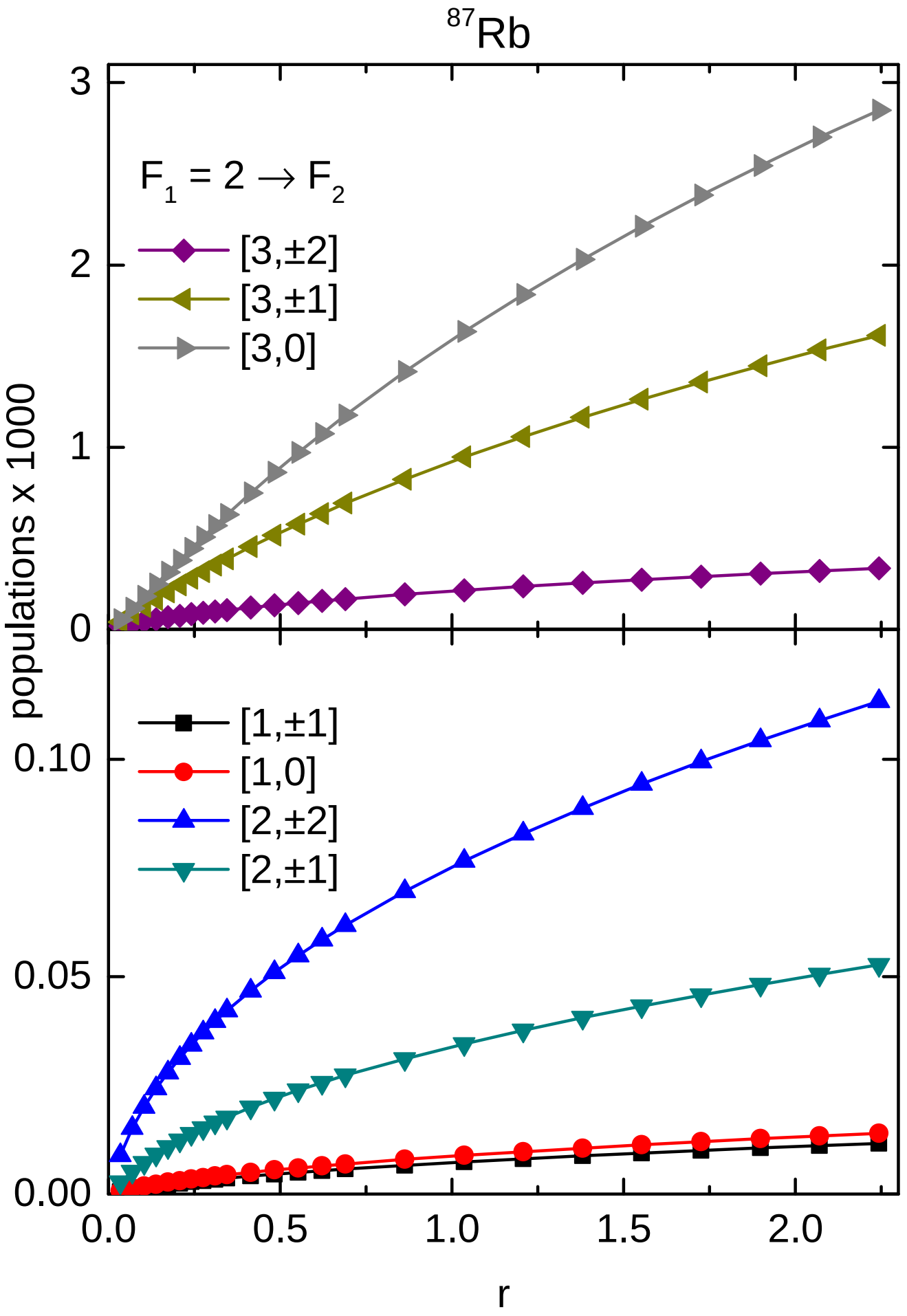

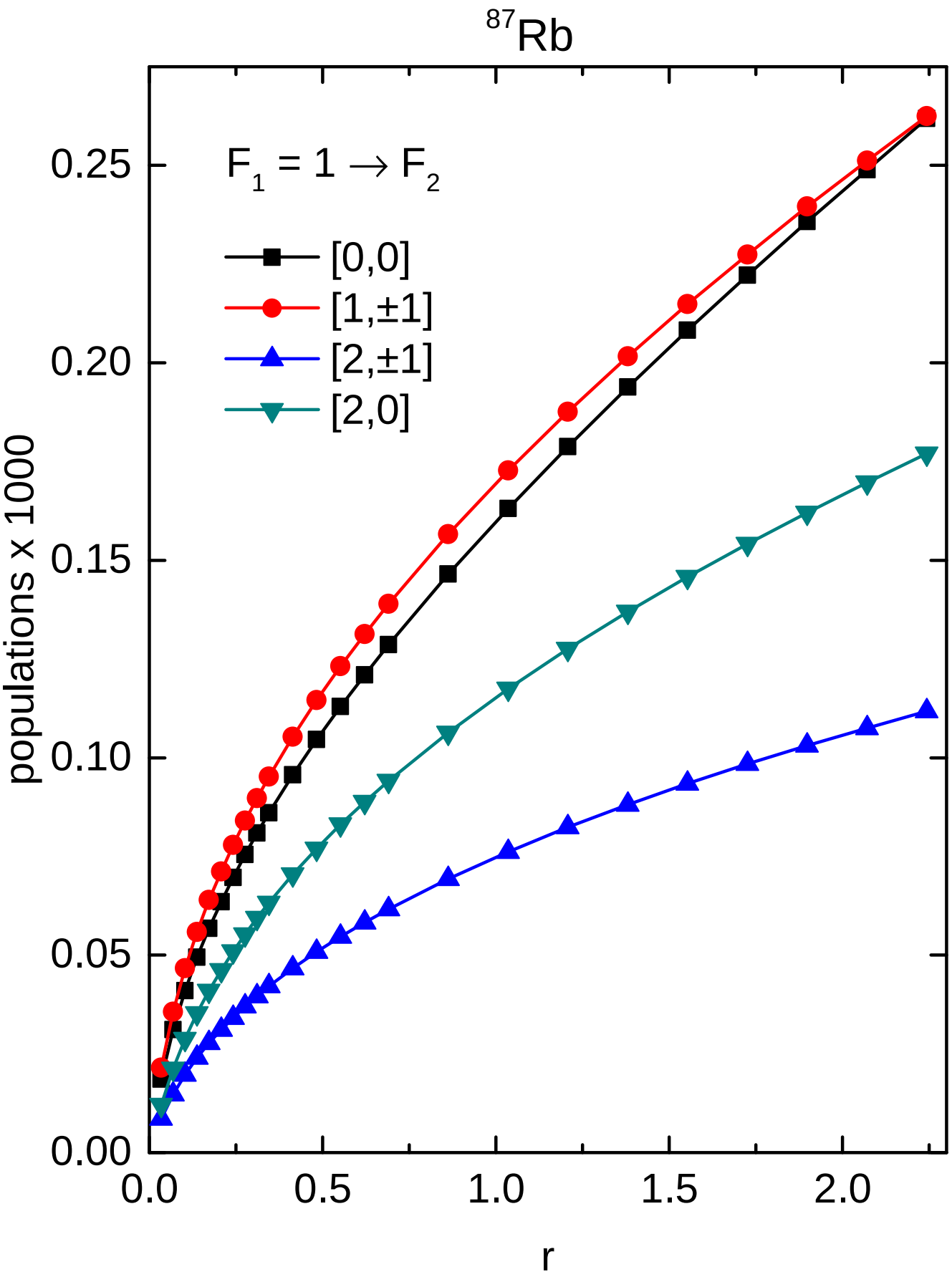

Figure 5

Click here to access/download;Figure(s);Rb87parpervelsel02.pdf

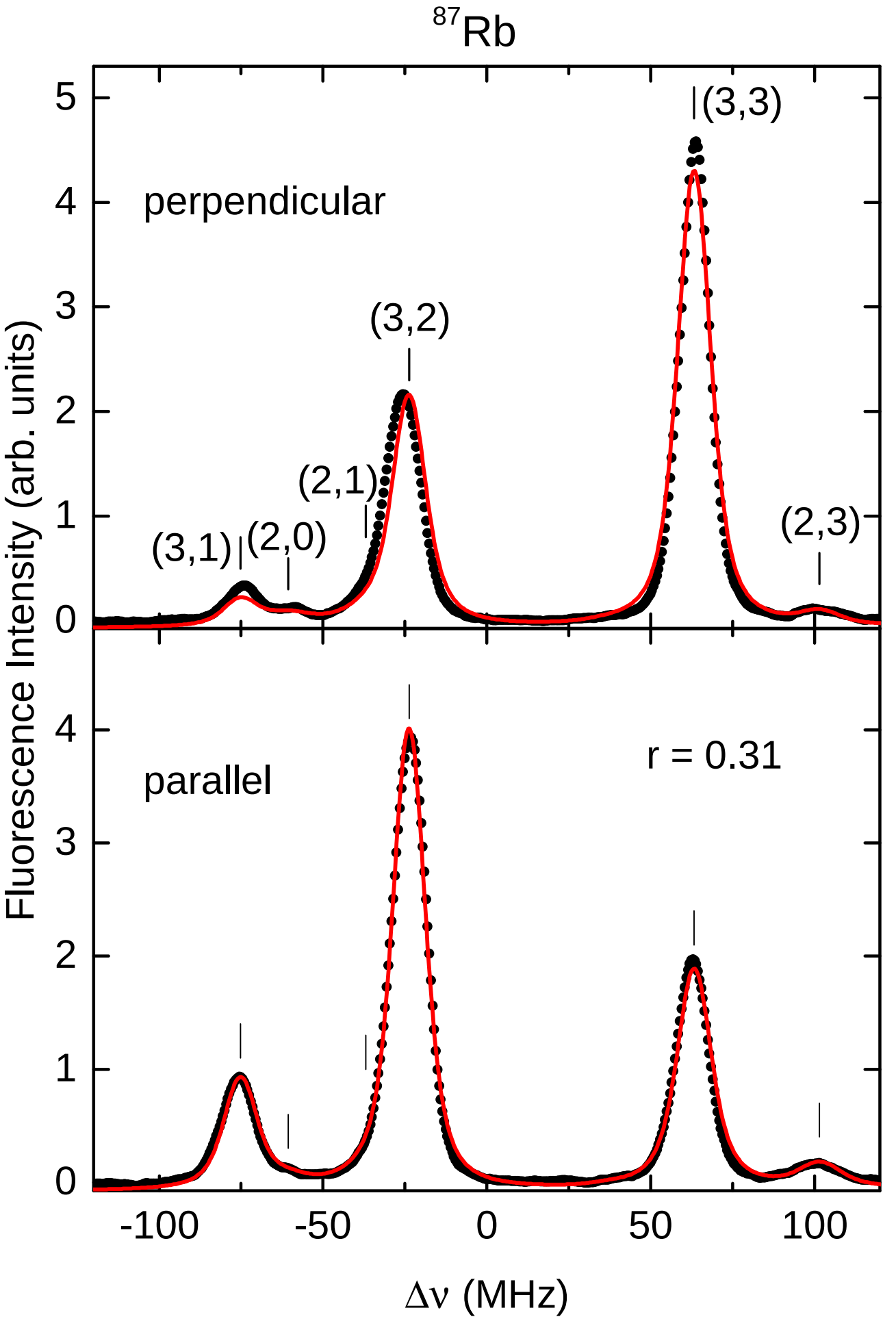

Figure 6

Click here to access/download;Figure(s);Rb85parpervelsel03.pdf

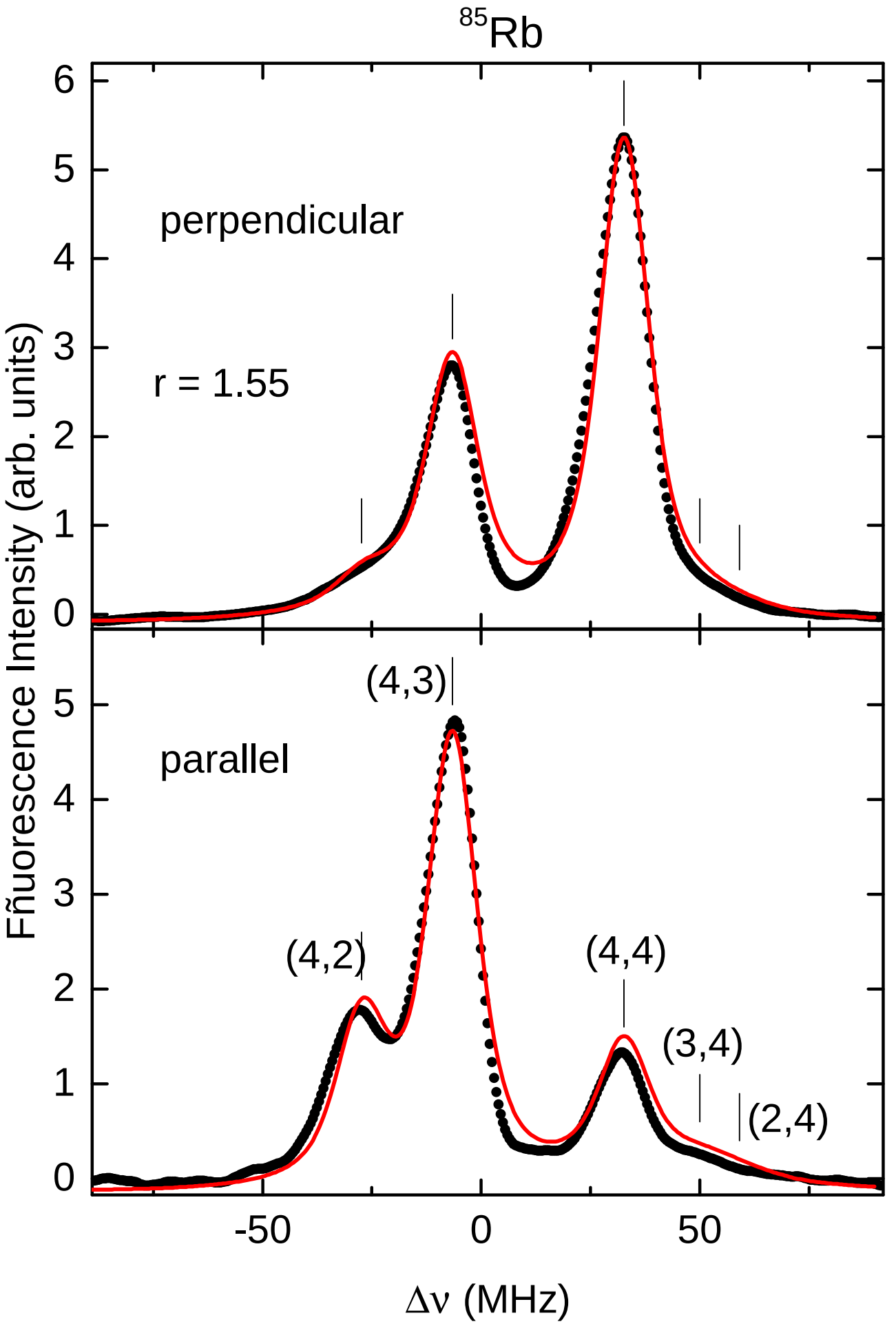

Figure 7

Click here to access/download;Figure(s);Rb85Hpape_917.pdf

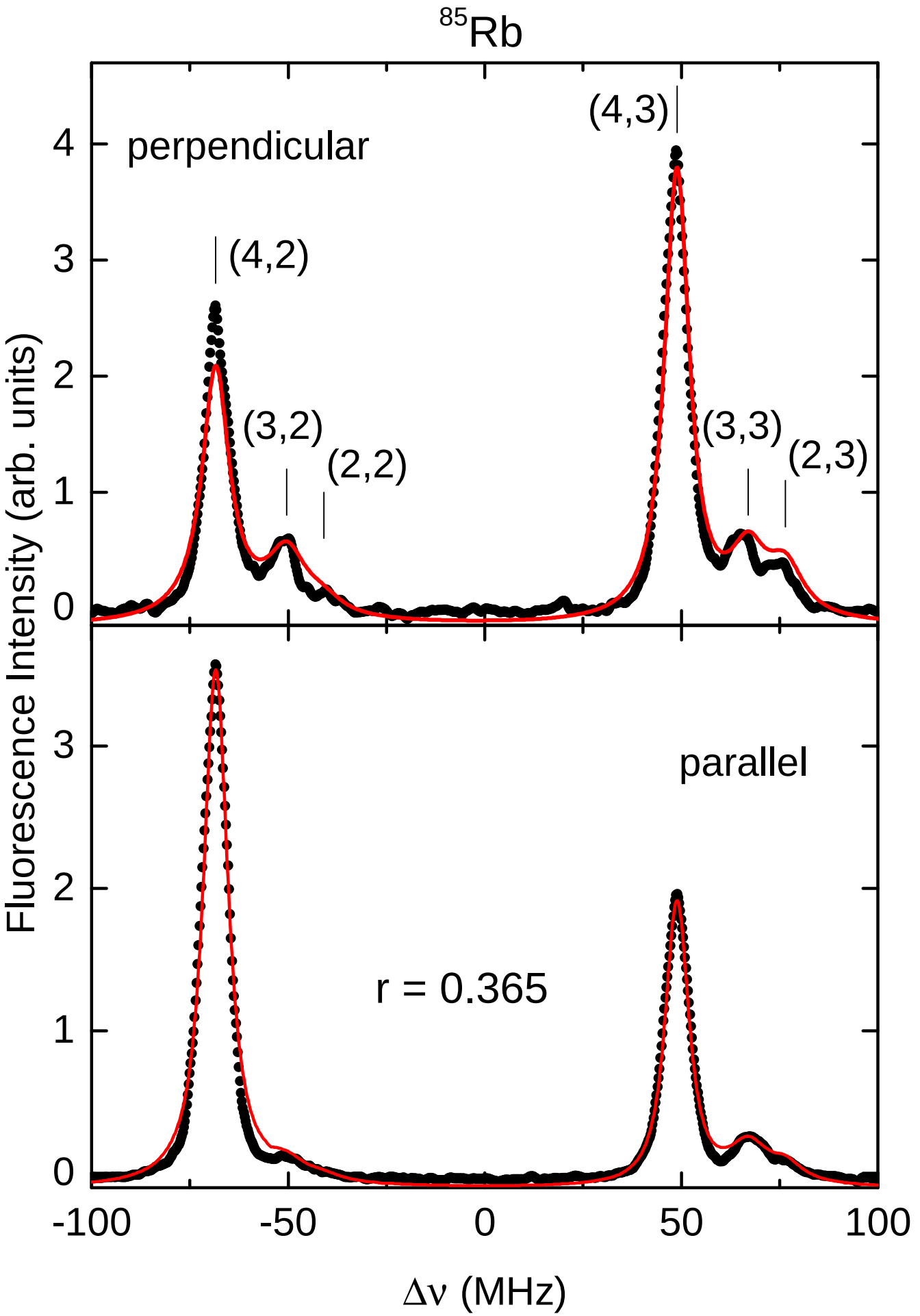

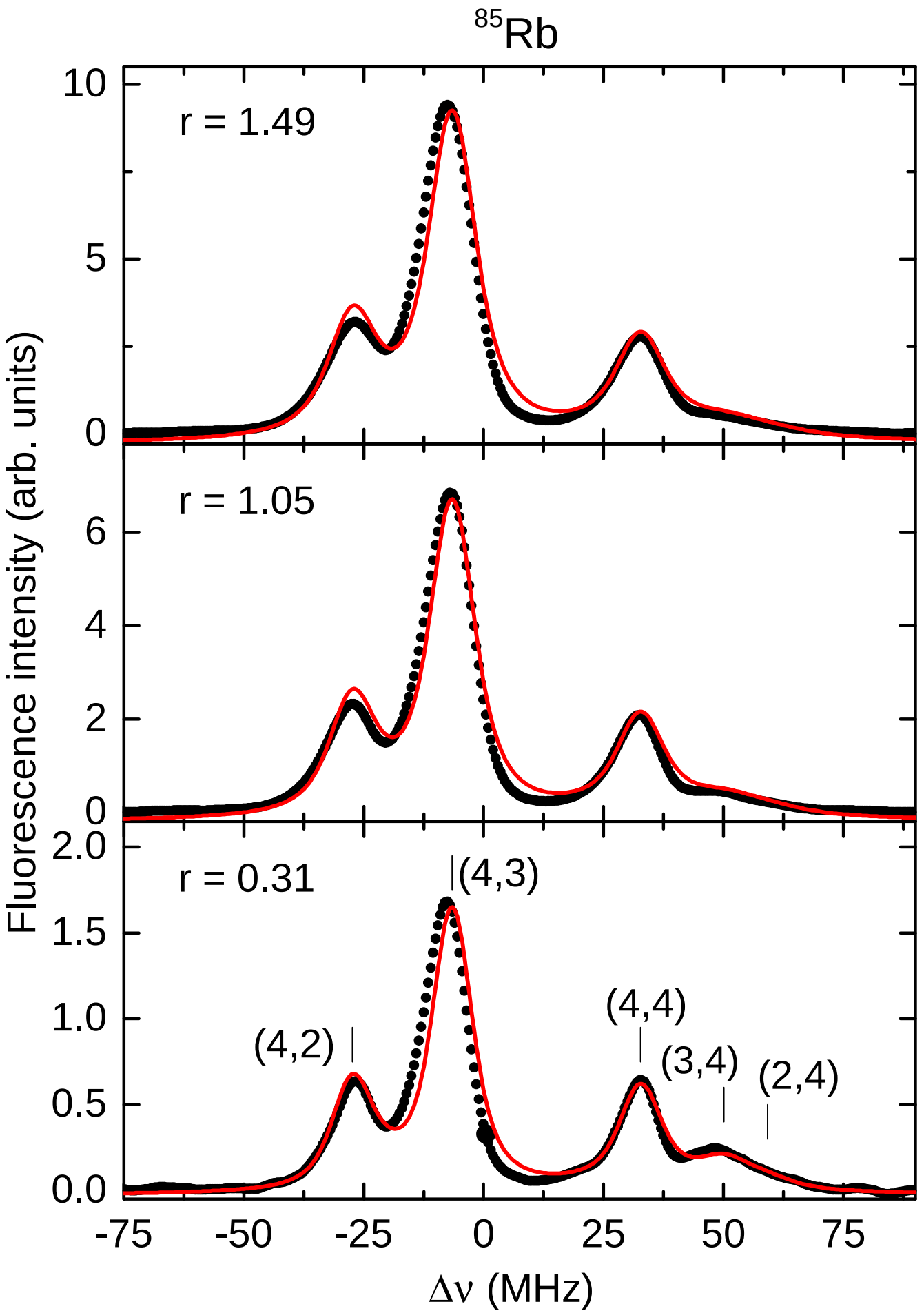

Figure 9

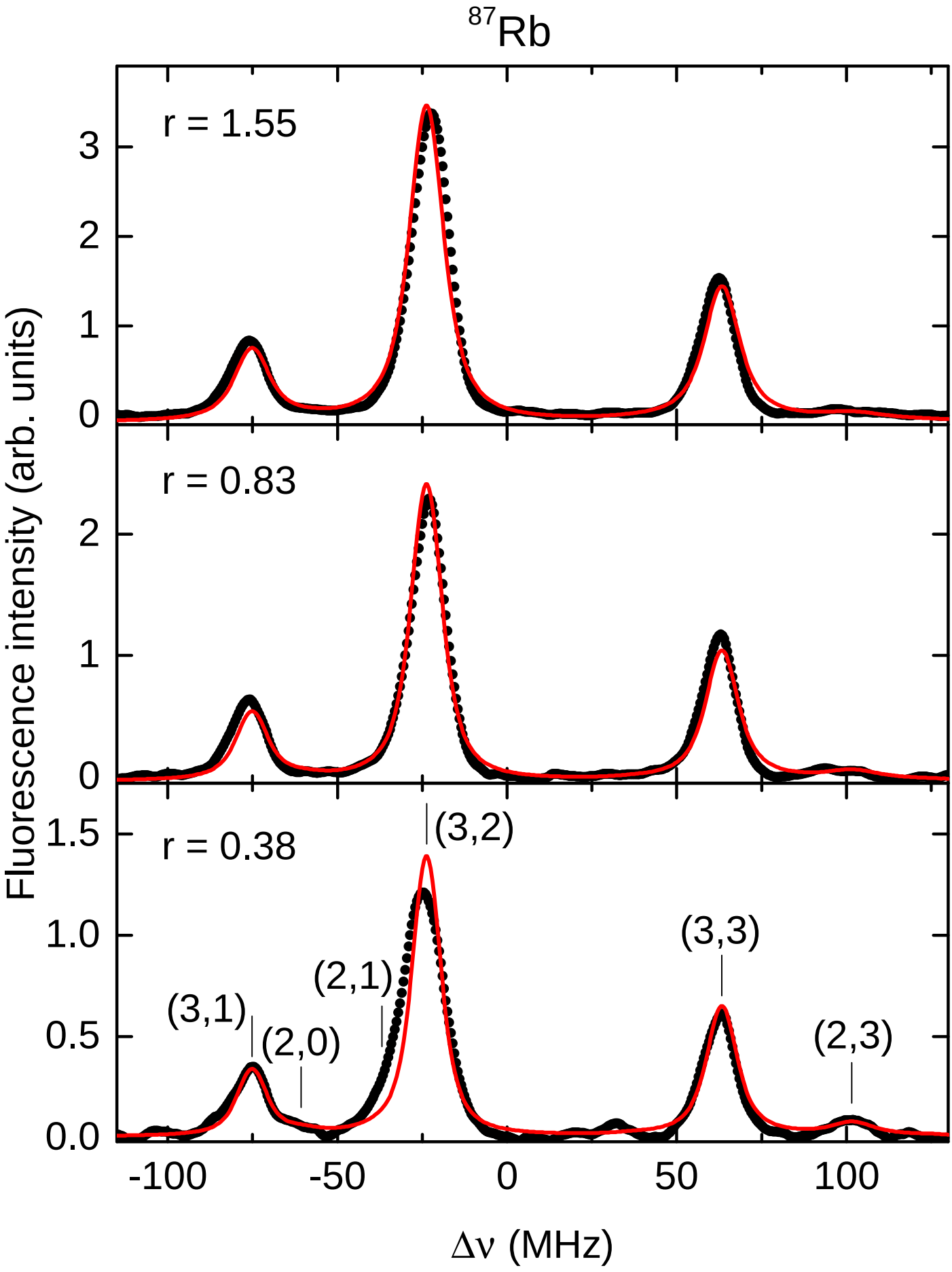

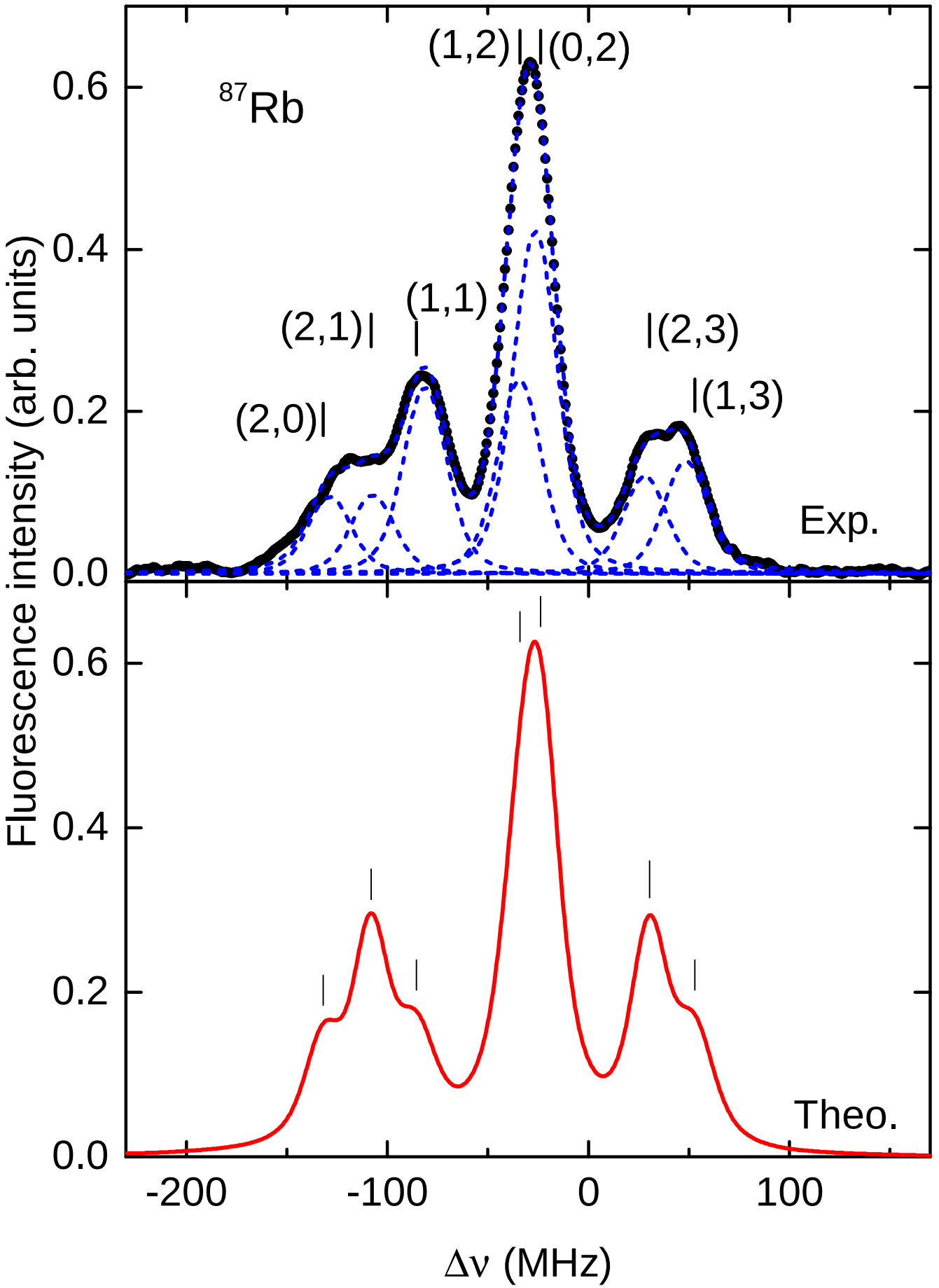

Click here to access/download

LaTeX Source Files

main.tex

Declaration of interests

☒The authors declare that they have no known competing financial interests or personal relationships that could have appeared to influence the work reported in this paper.

☐The authors declare the following financial interests/personal relationships which may be considered as potential competing interests: